OCEAN-ATMOSPHERE INTERACTION IN THE TROPICS

Peter J. Webster

Department of Meteorology
The Pennsylvania State University
University Park, Pennsylvania, USA

1. INTRODUCTION

1.1 The Signature of Water in Climate

Water imparts an indelible character on the climate of Earth. Although Earth is not the only planet in the solar system to possess water, it is unique since only Earth possesses vast reservoirs of liquid water in the oceans and suspended ice and droplet concentrations in the atmosphere. The consequences of water in the atmosphere are thus of fundamental importance, impacting both the long- and short-wave radiative streams as well as the planetary energy balance. Water acts simultaneously as the major greenhouse gas on the planet and as the major reflector of solar radiation. Collectively, the greenhouse and albedo effects produce an average surface temperature of Earth of about 33°C and ameliorate the diurnal and seasonal temperature ranges. Thus, through the agency of water in its many forms, the mean temperature of Earth has remained at about 15°C from the Cretaceous to present times within very tight margins allowing, in addition, a strong interactive biological system. Without an abundance of water in the Earth system, the average global temperature would reside nearer to –10°C and would probably be similar to a slightly warmer Mars.

The phase transients of water in the terrestrial temperature range are strong nonlinear functions of temperature. Given the spatial and temporal variation of temperature on Earth, a strong regionality of the type of phase change may be expected. Regionality in the distribution of water vapor may be seen in Fig. 1. The first panel plots the vertical distribution of the vapor pressure as a function of temperature for three northern hemisphere summer profiles at latitudes 0°N, 40°N and 75°N. The winter profiles are plotted on the second panel. The atmospheric pressure corresponding to each point is marked on the curves, and the saturated vapor pressure is plotted as the heavy solid line. The most prominent feature is that the tropics are considerably moister than the higher latitudes. For example, in

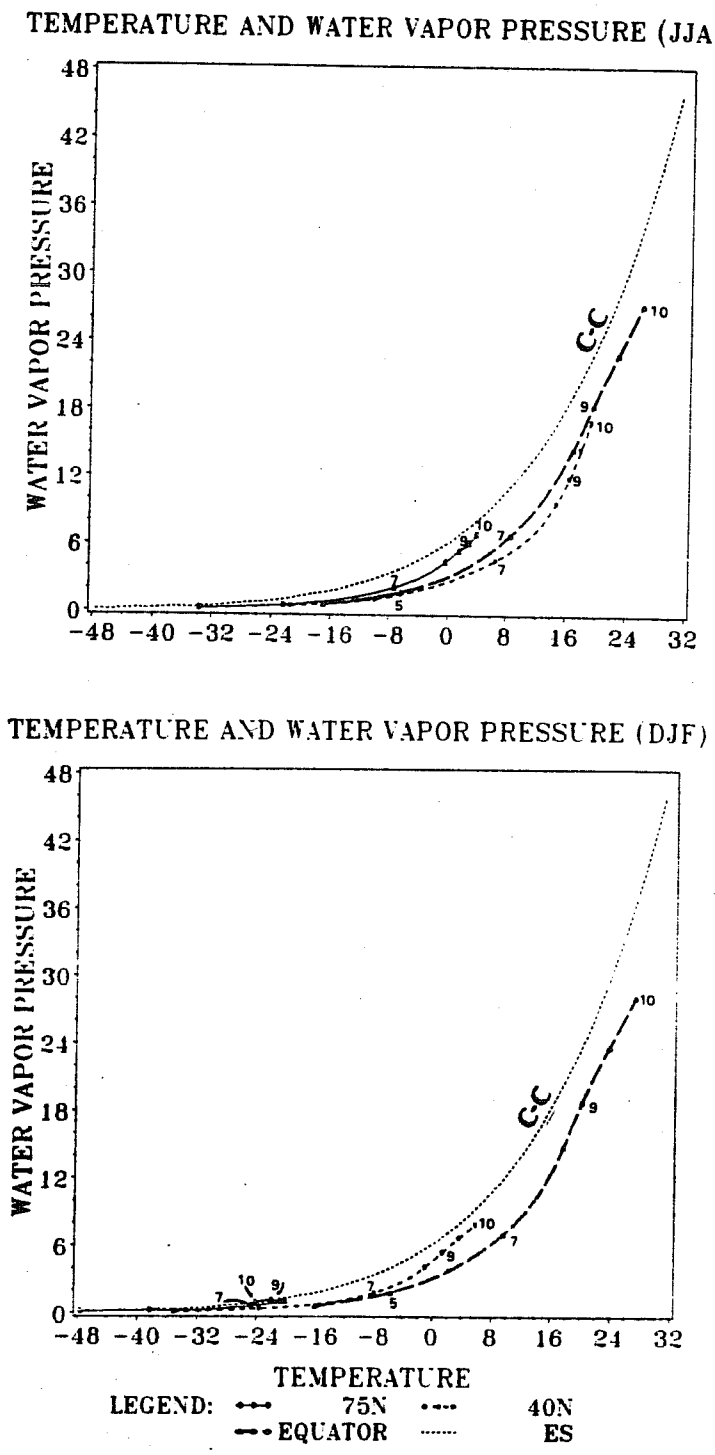

Figure 1: The atmospheric temperature (°C) versus vapor pressure (mb) for standard atmospheres at the equator (large dashes), 40°N (small dashes) and 75°N (solid) as a function of height (pressure levels marked) for (a) the mean boreal summer, and (b) the mean boreal winter. The left dashed line (marked C-C for Clausius-Clapeyron) is the saturation vapor pressure curve as a function of temperature.

winter the vapor pressure at the surface in the tropics is almost a factor of two greater than in the middle latitudes and an order of magnitude greater than in the polar regions.

The implications of the strong temperature dependency of vapor pressure are important for both radiative and latent heating effects. Atmospheric radiative absorbtion is a strong

function of water vapor concentration. Furthermore, reemission depends strictly on the amount and temperature of the vapor in a particular layer. The single scattering properties of cloud particles (i.e., optical depth, single scattering albedo and phase function) are a function of the amount of condensed water phase (i.e., solid or liquid) and particle size distribution. Collectively, these factors determine the albedo and emissivity of the atmosphere. Thus radiative effects of water in the atmosphere may be expected to vary in the atmosphere as a strong function of latitude.

In a similar sense to the radiative effects of water, latent heating of the atmosphere may be expected to have a distinct regional character. The amount of latent heat released for an equivalent amount of work in lifting a parcel of air through a column is also a function of temperature. Using Fig. 1 we can see that if a tropical parcel, initially residing in the lower troposphere, is raised (say) 1 km in the vertical, the amount of latent heat will be very much greater than at higher latitudes. The differences in latitude merely follow from the Clausius-Clapeyron relationship which governs the shape of the saturated vapor pressure as a function of temperature. That is, as temperature increases linearly, specific humidity increases exponentially. The heavy curve in Fig. 1 shows the saturation vapor pressure curve plotted against temperature. Clearly, the mean atmospheric curves follow the saturated curve to a close degree. Figure 2 shows the net temperature increase (i.e., the moist adiabatic temperature change less the adiabatic cooling) for parcels which, initially at 900 mb, are raised by 1 km. Mean northern hemisphere data was used. The temperature increase is plotted as a function of latitude and shows at least a three fold greater increase at low latitudes. For both the boreal summer and winter, the relative temperature changes induced by the latent heat release for an equivalent amount of work is at least a factor of two larger in the tropics than in the middle latitudes. Thus, convection in the warm pool regions of the deep tropics will be deeper and more intense and associated with the largest rainfall than at higher latitudes. Similar variations exist across the Pacific Ocean between the very warm western Pacific and the cooler eastern side of the basin.

Figure 3 provides a global perspective of the regionality of the hydrology cycle. The solid contours show the mean outgoing long-wave radiation (OLR; W m^{-2}) to space for the boreal winter season (DJF) as measured by satellite. The minimum values, for example, over the West Pacific and East Indian Oceans suggest that the emitting surface is very cold. This can only occur in the tropics if the emitting surface is a very deep cloud. As deep clouds are synonymous with precipitation, we may presume that minimum OLR regions are zones of precipitation. The dashed lines on the chart show sea surface temperature isopleths. A clear correspondence thus emerges between the two sets of isopleths. That is,

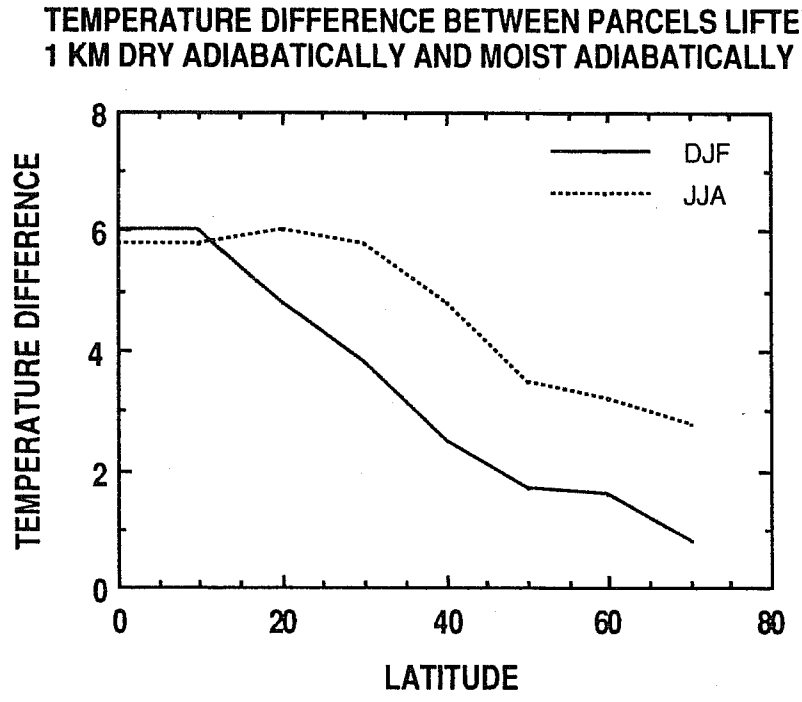

Figure 2: The net increase of temperature (ΔT) beyond adiabatic effects for raising a parcel 1 km. ΔT is plotted as a function of latitude for summer and winter. Note the large difference in temperature realized for the same amount of work close to the equator compared to higher latitudes. About a factor of two in ΔT also occurs between the warm pools of the western Pacific Ocean and the colder equatorial waters further east.

where the sea surface temperature is warmest, the OLR is lowest. By implication, warmest SST's correspond to the largest precipitation.

1.2 Hydrology and Modeling

(i) Tropical Land-Atmosphere Interactions

A number of studies have indicated the importance of hydrological effects in determining the nature of the general circulation and even controlling many aspects of the transient behavior of the atmosphere. For example, Shukla and Mintz (1982) showed that the rainfall over the continental regions could not be modeled properly without an adequate treatment of land hydrological processes including plant evapotranspiration. Webster (1983) and Srinivasan *et al.* (1990) have shown that the interaction between the land surface hydrology and the tropospheric heating is responsible for the subseasonal transient behavior of the monsoon. They found that if the ground hydrology were not interactive, then a steady state monsoon circulation is possible. However, with an interactive land hydrological processes,

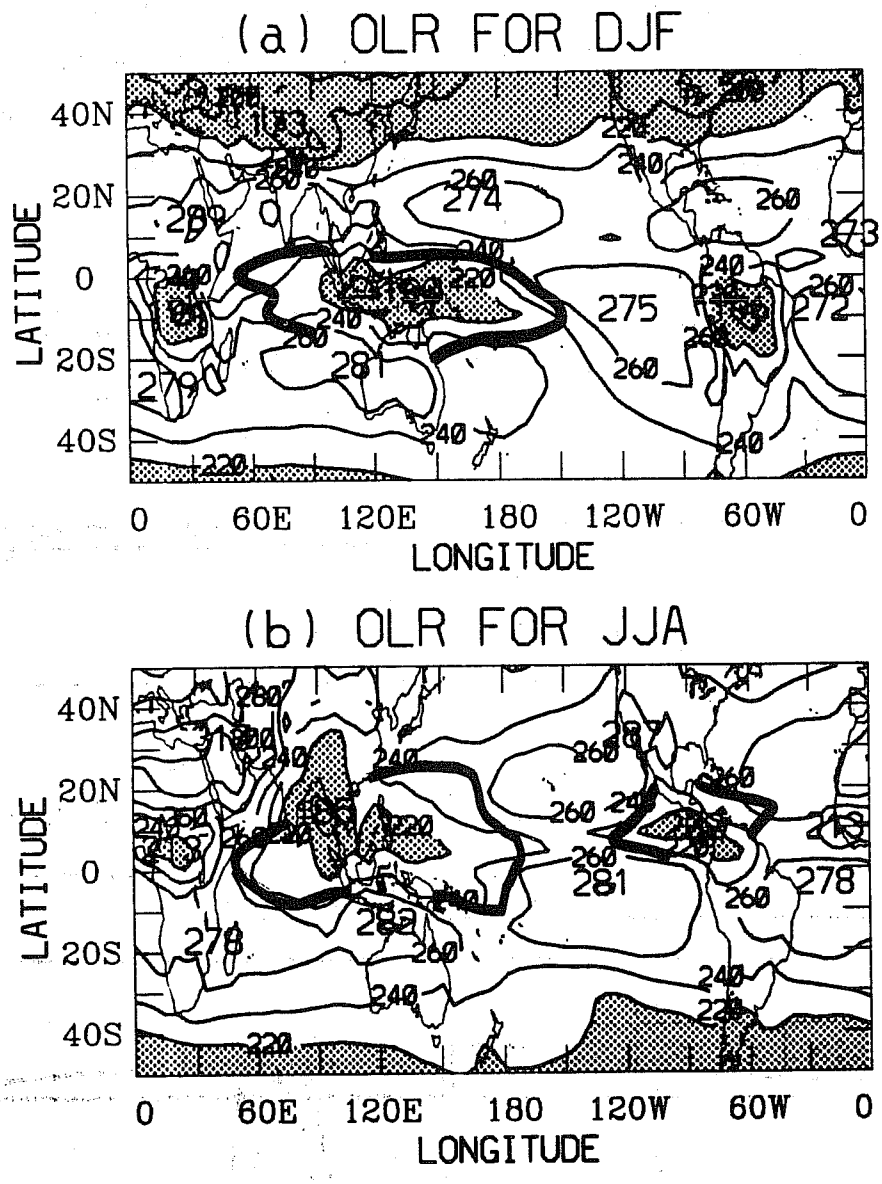

Figure 3: Mean outgoing radiation (OLR) for (a) June, July and August (JJA), and (b) December, January and February (DJF). Units are W m^{-2}. Heavy line represents the 28°C isopleth.

negative surface feedbacks continually displace the tropospheric heating maximum poleward. The effect is to create 30–40 day variability in the monsoon system.

A schematic diagram of the processes involved in the land-atmosphere interaction when a fully interactive ground hydrology is included can be seen in Fig. 4 (Srinivasan, *et al*, 1990). This figure shows a cross-section along a meridian across the equator and over South Asia and provides a description of the coupling of the ocean and the atmosphere through hydrological processes. Over the ocean, the surface temperature is determined by momentum transfer and turbulent mixing by the atmosphere together with the heat budget at the ocean surface. In regions where precipitation exceeds evaporation (i.e., $P\text{-}E > 0$), especially in the warm pool regions of the tropical oceans, the ocean can be stably stratified by the flux of fresh water. In turn, the stabilization alters the mode of interaction between

the ocean and the atmosphere. The stable layer prevents vertical mixing and blocks access to the cooler, fresher water below the thermocline. The fresh lens, so insulated, heats rapidly from solar radiation absorbtion and increases the fluxes of heat and moisture to the atmosphere. This interaction is the basis of the "barrier layer" theory of Lukas and Lindstrom (1987) which we will discuss later.

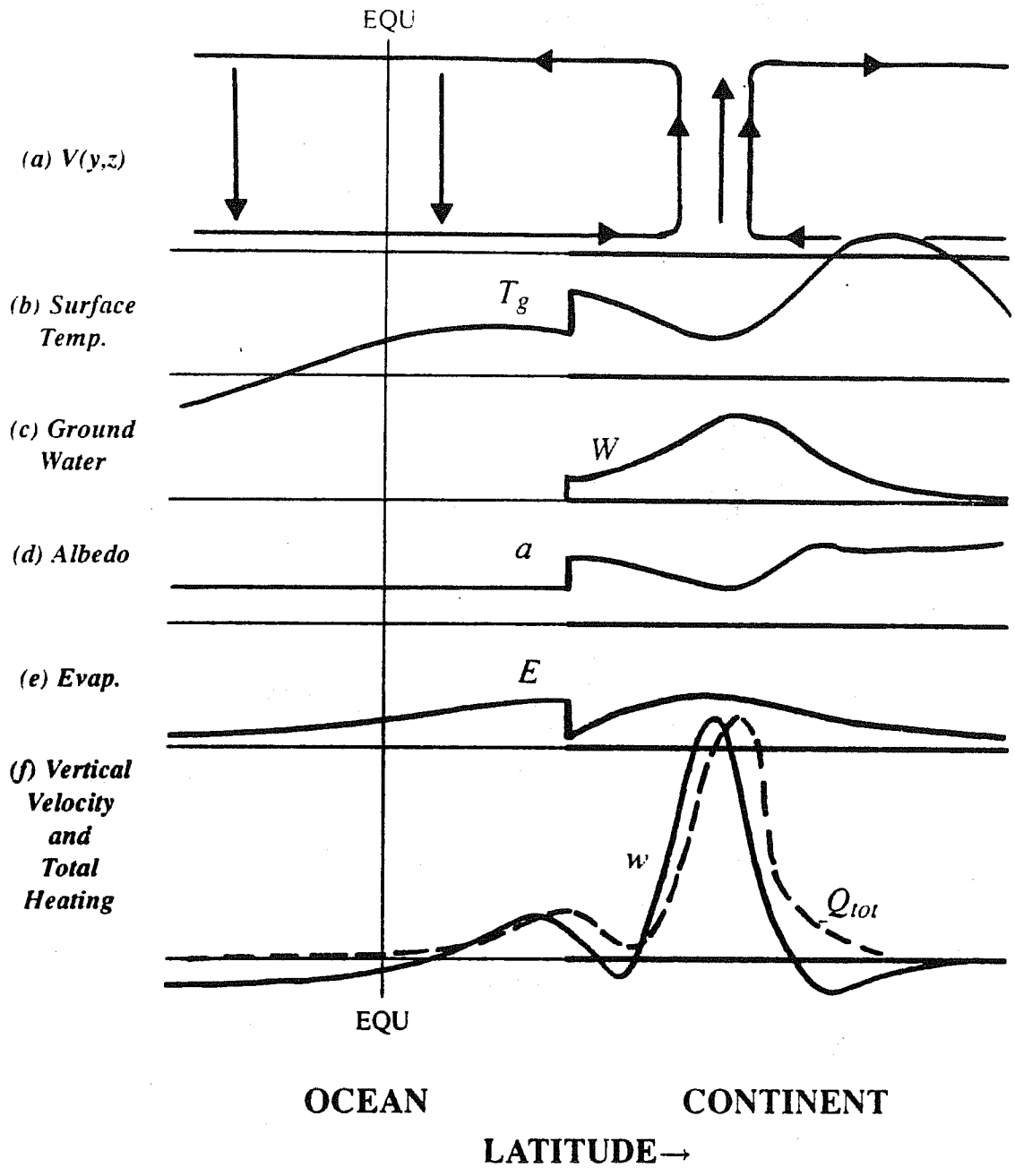

Figure 4: Schematic diagram of the interactive hydrology cycle over tropical land masses. Results from the simple monsoon model of Srinivasan, *et al* (1990) is used to indicate the degree of interaction between the atmospheric and surface hydrological processes. The figure shows the values of certain quantities as a function of latitude during the poleward propagation of a monsoon convective event. The quantities are: (a) a typical monsoon circulation with maximum ascending motion over the continent, (b) the surface temperature, (c) the ground water contained in the land surface, (d) the evaporation, and, (e) the total heating and vertical velocity in the atmospheric column. Srinivasan, *et al* (1990) contend that the impact of the ground hydrology is to slightly offset the vertical velocity and total heating which causes poleward propagations of the convection.

Over tropical continental regions, the hydrological processes are even more complicated. In the vicinity of the region of maximum rising motion, the surface temperature is a minimum and the evaporation is a maximum. Precipitation and ground water also possess maximum values and the ground albedo has a local minimum. In the bottom panel, it can be seen that the vertical velocity and the total heating are out of phase. Webster (1983) and Srinivasan *et al* (1990) show that the phase difference is a direct result of the interactive ground hydrology. With an interactive ground hydrology, the monsoon goes through a series of northward migrations similar to those documented by Sikka and Gadgil (1980).

(ii) Ocean-Atmosphere Interaction

The hydrology cycle has a significant impact on the interactions between the ocean and the atmosphere. Traditionally, the coupling of the ocean and the atmosphere has been thought of in terms of two simple processes. The ocean is driven by a momentum flux from the atmosphere. The atmosphere, in turn, is driven by the heat flux (latent and sensible) from the ocean. However, in certain regions the interaction may be considerably more complex. Figure 5 shows a schematic diagram of the coupled ocean-atmosphere system where the atmospheric part of the hydrosphere (clouds, precipitation and the ambient moisture distribution) is allowed to fully interact with the radiation field, both within the atmosphere and the ocean, and with the density structure of the ocean's upper layer. The ocean-atmosphere interaction through stress and surface fluxes still possesses a basic importance, but now the hydrology cycle has the potential of modifying significantly the basic driving mechanisms of the coupled system. In the following paragraphs we will show that the difference of the radiative flux divergence between cloudy and clear regions provides a radiative heating gradient (∇Q_{rad})[1] which is of the same sign and about 30% to 50% of the magnitude of the latent heating gradient (∇Q_{lh}).

(iii) Hydrological Processes in Ocean-Atmosphere Interaction

Variations in the radiative fluxes associated with the hydrological cycle are probably of greater importance than previously realized. Ramanathan (1987) estimated that the differential heating caused by the depleted net radiation at the ocean surface due to cloudiness differences between one side of the equatorial Pacific Ocean and the other is about 1°C/month averaged through the first 100 m of the ocean. The cloud structure may

[1] Specifically, ∇Q_{rad} refers to the horizontal gradient of the vertical flux divergence of net column radiation.

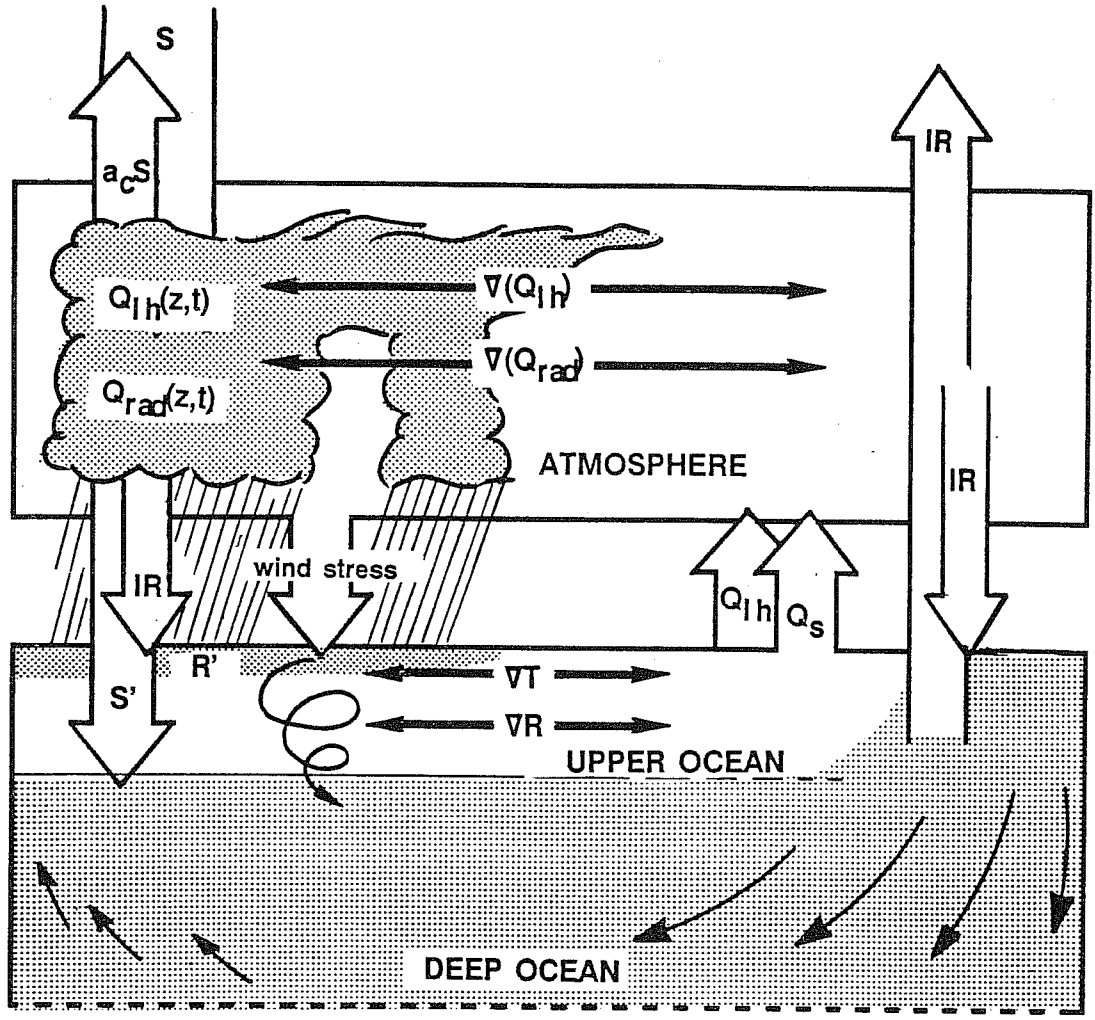

Figure 5: Schematic view of the coupled ocean-atmosphere system, where, in addition to the traditional momentum and heat flux driving of the system, the hydrology cycle is completely interactive. The implications of the differences between the traditional and this system are discussed in the text. It is argued that the active hydrology components of the system are zero order.

also influence the vertical heating distribution in the ocean by changing the proportion of infrared and solar radiation. Stephens and Webster (1979) showed that the impact of clouds was very complicated and varied considerably from one location to another. At higher latitudes, where the sub-cloud layer is dryer in comparison to the tropics, the downwelling IR from the cloud is an important component of the surface energy balance and offsets, to a large degree, the reduction in solar radiation (see Section 3.1). But, despite this offset, the attenuation of the radiation with depth in the upper ocean is very different between clear and cloudy days as the long- and short-wave streams have vastly different attenuation scales in water (see Section 3.2(i)) However, at low latitudes, the extremely moist boundary layer impedes the downward flux so that the apparent radiating surface at the ground may be well below the cloud base. Thus, the impact of cloudiness in the tropics is mainly to reduce the intensity of the solar stream (Stephens and Webster, 1979).

It should be noted that the ocean surface layer heating gradient imposed by the cloudiness difference is in the opposite sense to the atmospheric radiation and latent heating gradients. However, the severely depleted solar beam below the convective regions causes upper ocean cooling. Ramanathan (1987) estimated that the cooling may be about 1°C/month. Such cooling may cause ocean-atmospheric feedbacks which may cause the warm water, and consequently, the convection, to move progressively eastward. The ocean buoyancy flux is a strong function of the net heating at the ocean-atmosphere interface as well as the fresh water flux into the ocean. The induced density gradients may drive anomalous currents which may be important on interannual time scales. The key to the coupling comes from the sensitivity of the atmosphere to small changes in surface temperature where the sea surface temperature is warmest. Palmer and Mansfield (1984) have shown that the atmospheric anomaly induced by a 1°C change of SST in the West Pacific is much larger than that produced by a 4°C change in the East Pacific where the background SST is much cooler.

In the following paragraphs, we will investigate a number of processes which influence the interaction of the ocean and the atmosphere. The processes considered are:

(a) Cloud and the total surface radiation flux at the ocean surface,

(b) The impact of cloud on the vertical heating distribution in the upper ocean,

(c) Precipitation and fresh water input into the ocean,

(d) Episodic heat, moisture, fresh water and momentum fluxes from the atmosphere to the ocean associated with convective tropical disturbances, and,

(e) Clouds and total diabatic heating in the ocean-atmosphere system.

In a final section, a conceptual model of the coupled ocean-atmosphere system will be developed which extends the role of hydrology from the short times scales which are the major focus of the earlier sections to very much longer time scales. It will be argued that even on these extended periods, the hydrology cycle is of critical importance in placing narrow bounds on climate.

2. ROLE OF HYDROLOGY IN OCEAN AND ATMOSPHERE DYNAMICS

Figure 6(a) shows the long-term average boreal winter (DJF) and summer (JJA) SST distributions corresponding to non-El Niño periods in the Pacific shown in Fig. 3. The heavy isopleth in Fig. 6(a) corresponds to the 28°C isotherm. The most intriguing feature is that OLR minima (and, thus, precipitation maxima) correspond to SST maxima. Figure 6(b) (Lau and Chan, 1988) shows the variance of the OLR in the 1-5 day period band

for JJA and DJF. Figure 6(c) shows the same variance but in the 40-50 day period band. Clearly, the majority of the tropical convection on transient time scales lies within the 28°C isotherm, or in the case of the higher frequency band, over the tropical continents. It appears that it is the aggregate of these convective transients that form the long-term diabatic heating gradient across the tropical oceans.

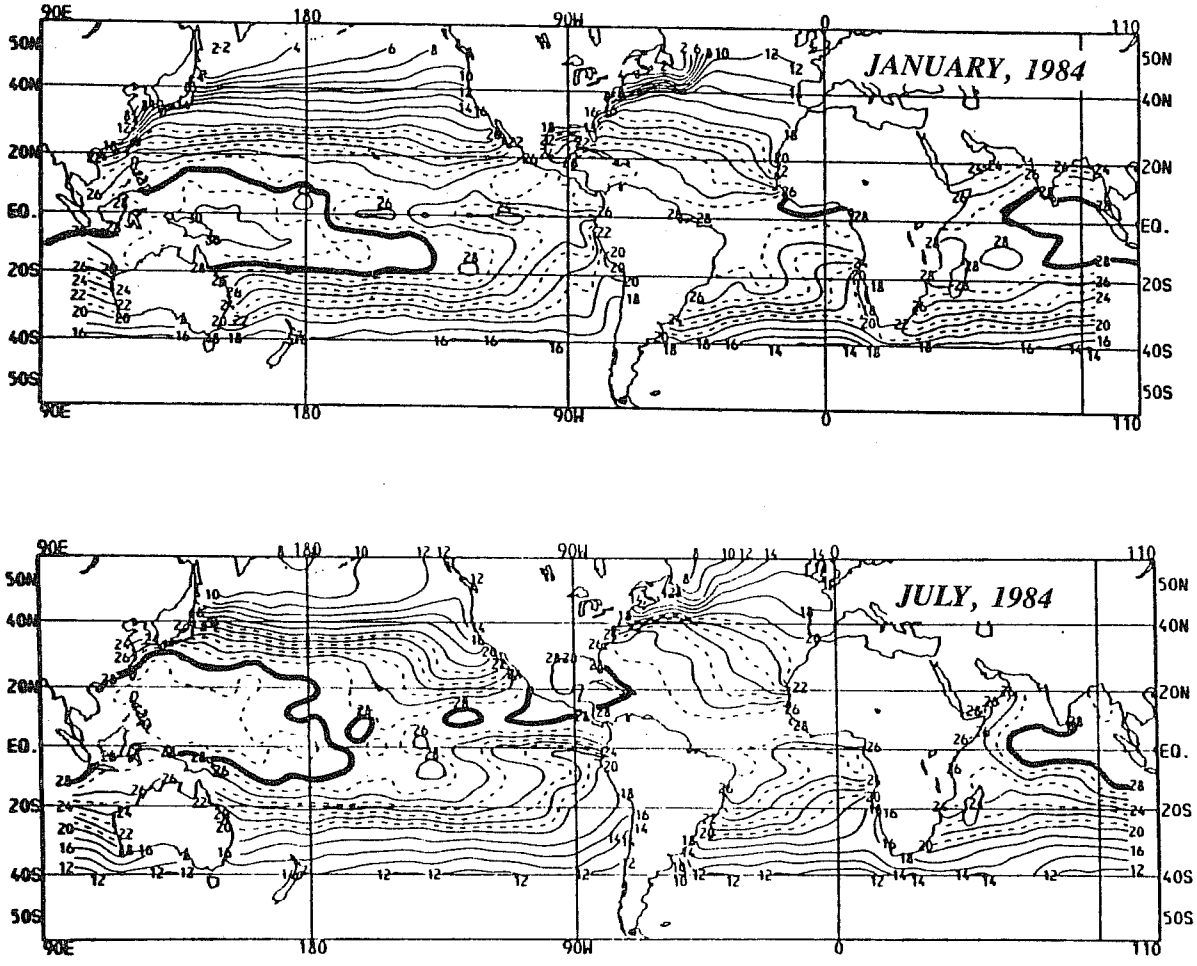

Figure 6(a): Sea surface temperature distributions for the January, 1984 (upper panel) and July, 1984(lower panel). Heavy line depicts the 28° isotherm.

2.1 Basic Structures of the Tropical Atmosphere and Hydrology

In the tropical oceans, deep organized convection tends to fall within the 28°C sea surface temperature isotherm as shown in Fig. 3. The warm SST-convection juxtaposition remains a mystery. Many attempts have been made to show that 28°C is the threshold temperature at which some instability arises. However, we will now argue that the physics that control the SST-convection relationship are a result of the normal modes of the tropical atmospheric and the moist thermodynamics of the hydrology cycle.

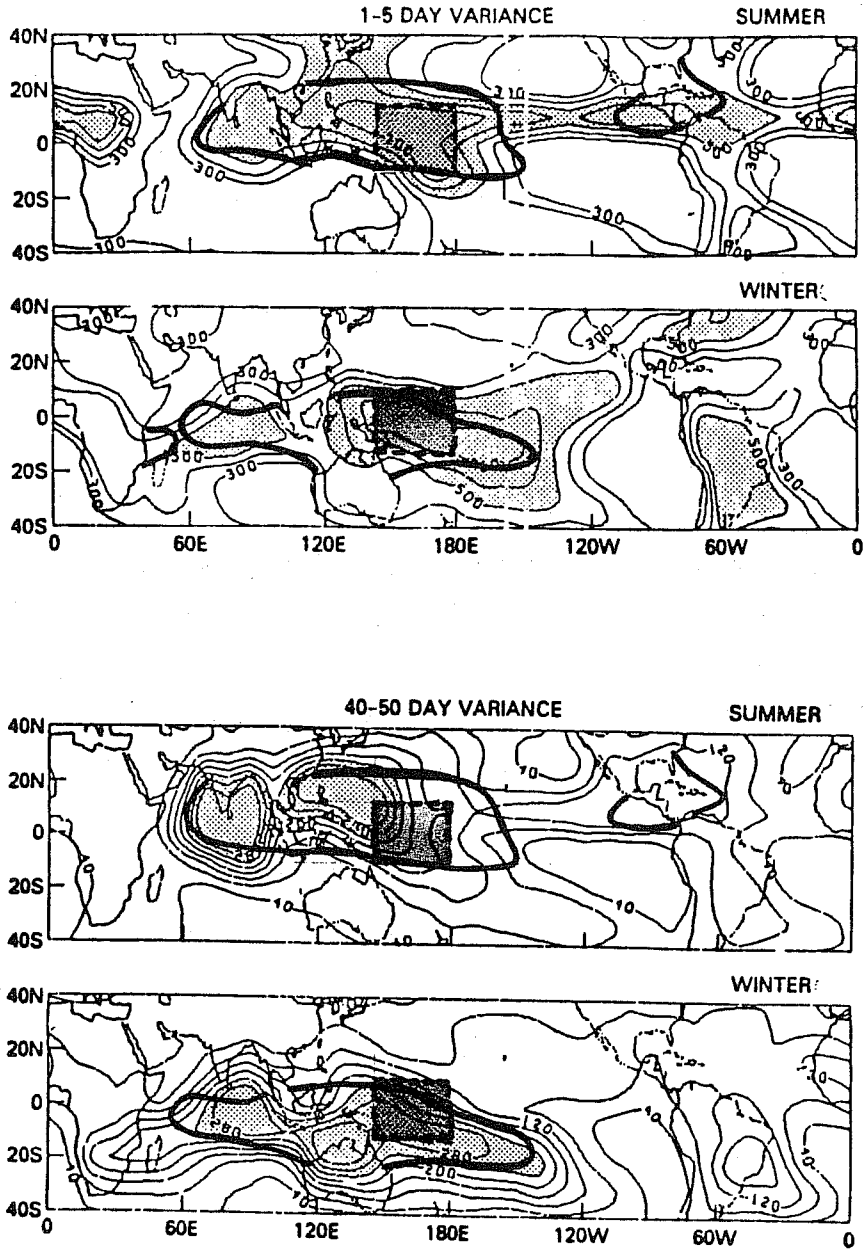

Figure 6(b): Distribution of the variance of OLR in the 1–5 day band for the boreal summer (upper panel) and the boreal winter (lower panel). After Lau and Chan (1988). (c) Same as Fig. 6(b) except for the 40–50 day band. After Lau and Chan (1988).

Figures 7(a) and (b) describe the relationships between convection and the sea surface temperature portrayed as a schematic sequence. Consider two regions (e.g., the western and eastern Pacific Ocean) with temperatures T_1 and T_2 where $T_1 > T_2$ and $T_1 \approx T_{max}$ where T_{max} is the maximum ocean SST[2]. The following paragraphs define the important processes responsible for the juxtaposition of convection and the warmest sea surface temperature. The first panel of Fig. 7(a) shows Clausius-Clapeyron relationship where the saturation vapor pressure, e_s is plotted as a function of T. The nonlinearity of the relationship insists that $e_s(T_1) >> e_s(T_2)$. If we take representative temperatures of the eastern and western

[2] The warmest SST's are observed in the warm pool regions of the tropical oceans. Temperatures rarely exceed 29–30°C. However, the warmest SST's exist over the Arabian Sea and the Bay of Bengal during late spring before the onset of the Asian monsoon. Temperatures of 30°C are common over wide areas.

Pacific as 20°C and 29°C, we find that $e_s(29°C)/e_s(20°C) \approx 1.7$. Thus, we might expect that moist processes will be considerably more important in the warm pools. We can see the implications of the nonlinearity of the moist processes by calculating the equivalent heat content in various parcels if they were to completely condense their water vapor. Defining the free convective height of a moist parcel as the level at which a parcel has expended its latent heat, or, equivalently, the level at which its lapse rate asymptotes to dry adiabatic during ascent. Assuming that the parcels were initially saturated we find that the free convective height is a strongly nonlinear function of the surface temperature. The second panel shows a plot of the free convective height as a function of SST. If the magnitude of the latent heat release is a function of the surface e_s then the distribution of the heating in the vertical is given by the convective height in the particular column. Thus, the warmer moister column will have a higher and larger maximum latent heating rate than its cooler dryer neighbor. The third panel shows a schematic representation of the heating profiles associated with columns T_1 and T_2. In essence, the SST determines the magnitude of the latent heating and also the height of its maximum.

Figure 7(b) shows the consequences of the different heating profiles. In an equatorial easterly basic flow, the principal mode that will be excited is the equatorial Kelvin wave. The mode closest to resonance is the gravest horizontal mode (Webster, 1972) Thus, assuming a white noise forcing distribution, a planetary scale response in longitude may be expected. The magnitude of the response depends on the amplitude of the forcing. However, the vertical scale of the Kelvin mode depends on the vertical scale of the heating, as this will determine the structure of the viscous wave (Chang, 1977) or the height to which cumulus mixing will occur. Thus, even though the horizontal scales relative to the forcing in the two columns may be the same, the vertical scale is very different (upper panels). Thus, the Kelvin wave in the cooler column must grow within a strong subsident region, forced by the dominant Kelvin mode associated with the higher and stronger heating distribution of the warmer column. In other words, the Kelvin wave associated with the warmest sea surface temperature regions will dominate over all other tropical modes controlling the latent heating distributions (middle panels). The last panel of Fig. 7 (b) shows the latent and radiative heating profiles that may be expected in the two columns. In Section 3.5 we will show that the gradients of radiative heating and latent heating are always of the same sign.

In summary, it is suggested here that the only special feature of the 28°C isotherm in the SST-convection relationship is that it is within a degree or so of the maximum ocean temperature observed on Earth.

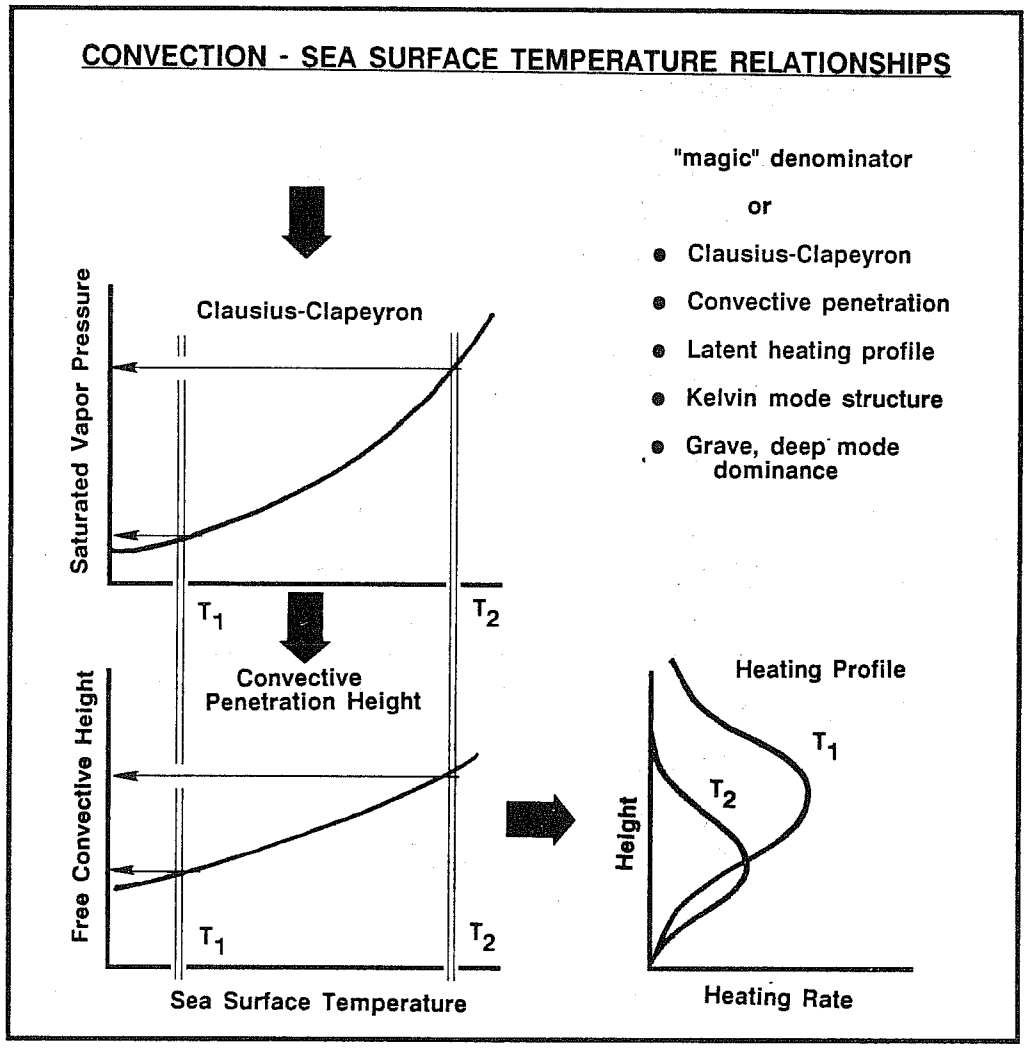

Figure 7(a): Schematic sequence attempting to relate the distribution of organized convection over the oceans with sea surface temperature. The first panel shows the Clausius-Clapeyron relationship ($e_s = e_s(T)$) and its relationship to the free convective height in the atmosphere (panel 2) representing the atmosphere over the warm pool regions of the western equatorial Pacific and the cooler waters of the eastern Pacific. Two columns are considered with temperatures T_1 and T_2 where $T_1 < T_2$. Assuming the same vertical distribution of relative humidity in the two columns, and assuming that convection occurs, the heating profile associated with warm column would be higher and stronger.

2.2 The Slowly Evolving Basic State at Low Latitudes

Figure 8 (from Webster, 1983) shows two schematic cross sections along the equator representing the flow in the longitude-height plane for the two climate epochs associated with large positive and negative values of the Southern Oscillation Index (SOI)[3] which correspond to cold (La Niña) and warm (El Niño) events in the tropical Pacific Ocean. The stippled area denotes sea surface temperatures greater than 28°C. Over this warm pool are regions of mean ascending air, which, together with the ascent over the continents, form a series of east-west cells along the equator (or "Walker Circulations") which were identified

[3] Defined here as the normalized difference in surface pressure between Tahiti and Darwin.

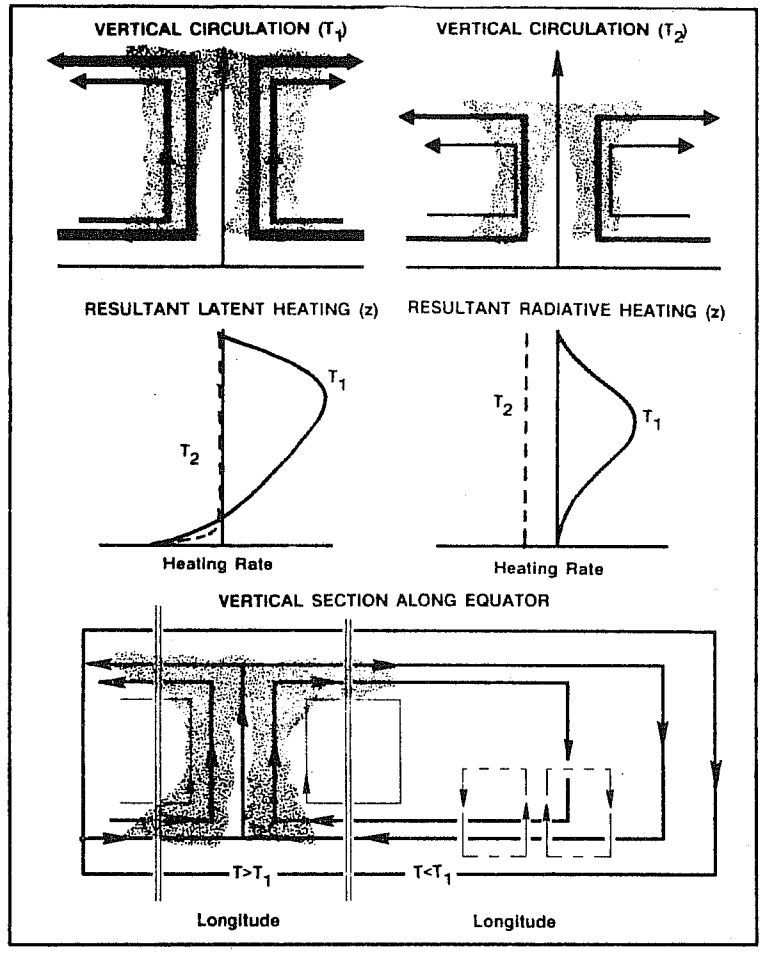

Figure 7(b): Consequences of the higher and stronger heating profile in the warm column will be to produce a stronger and deeper viscous equatorial Kelvin mode than that produced in the cooler column (upper panels). Although both may be expected to possess a planetary longitudinal scale, the convective mode in the cooler column would have to develop in the subsidence of the warmer mode (middle panels). Thus, the warm region Kelvin mode will dominate over incipient convection elsewhere (middle panels). The last panels show the final latent and radiational heating profiles. With the development of convection, the resultant radiative flux divergence "locks in" the total diabatic heating gradient. The fact that the radiational heating gradient is the same sign as the latent heating gradient will be discussed in detail in Section 3.5. Thus, the significance of the 28°C isotherm and its relationship to organized convection is that the isotherm is very close to the maximum SST and, thus, is associated with the strongest and deepest convective modes.

observationally by Krishnamurti (1971). These Walker Circulations are the manifestations of the dominant normal modes in the equatorial wave guide (Webster, 1972: Gill, 1980).

Comparing the El Niño and La Niña situations, it is obvious that the location of the cells and their associated easterlies and westerlies possess considerable interannual variation. Theoretical explanations of the mean tropical circulation, in which the cells are described as stationary or steady state trapped equatorial modes forced by latent heating gradients, associated with the gradient of sea surface temperature across the tropical oceans, were put forward by Webster (1972, 1973) and Gill (1980). The Walker Circulation described in Fig. 8 represents a slowly evolving basic state with which all transient motions on time scales

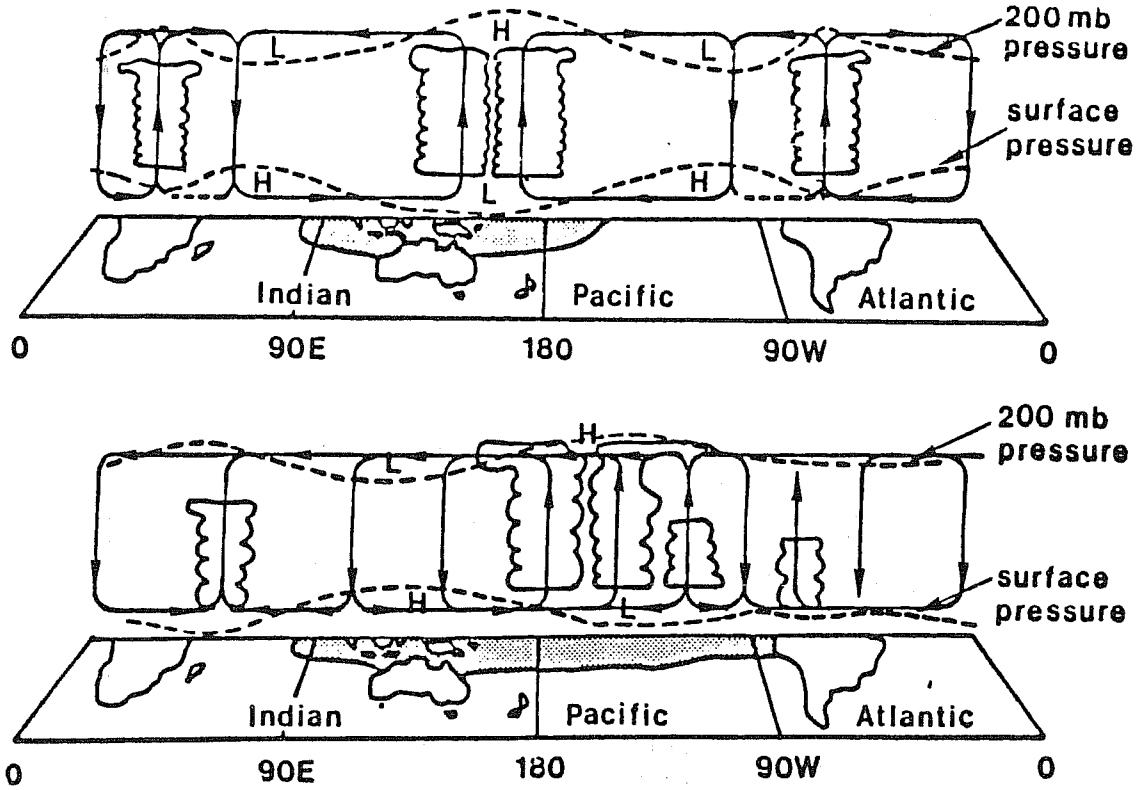

Figure 8: Schematic diagram of the zonal circulations ("Walker Circulations") along the equator during periods when the SOI ≥ 0 (upper panel) and SOI $<< 0$ (lower panel) (Webster, 1983; Webster and Chang, 1987).

less than seasonal or interannual must contend.

2.3 Relationships Between the Slowly Evolving Basic State, Transients, Sea Surface Temperature and the Hydrology Cycle

Figure 9 (Webster and Chang, 1988) shows sections along the equator of the long-term averages of the zonal wind component (U,m s^{-1}), the *OLR* equivalent temperature (K) and the perturbation kinetic energy (*PKE*) where $PKE = \left(u'^2 + v'^2\right)/2$ and u' and v' are the temporal deviations of the zonal and meridional velocity components. Clearly, minimum *OLR* (and maximum convection) corresponds to minimum *PKE*. At first inspection it would appear odd that the region of mean and transient maximum convection, which we know to lie within the 28°C isotherm, does not correspond to the region of maximum *PKE*. Indeed, Arkin and Webster (1985) showed that maximum *PKE* was colocated with the regions of maximum westerlies in the upper troposphere over the central and eastern Pacific Ocean and the mid-Atlantic Ocean and that these regions possessed convective minima.

There are three hypotheses which attempt to solve the convection-PKE paradox. They all are relevant to the dynamics of teleconnections which relate the tropical heating to the circulation of the global atmosphere. The "westerly duct" theory considers the role

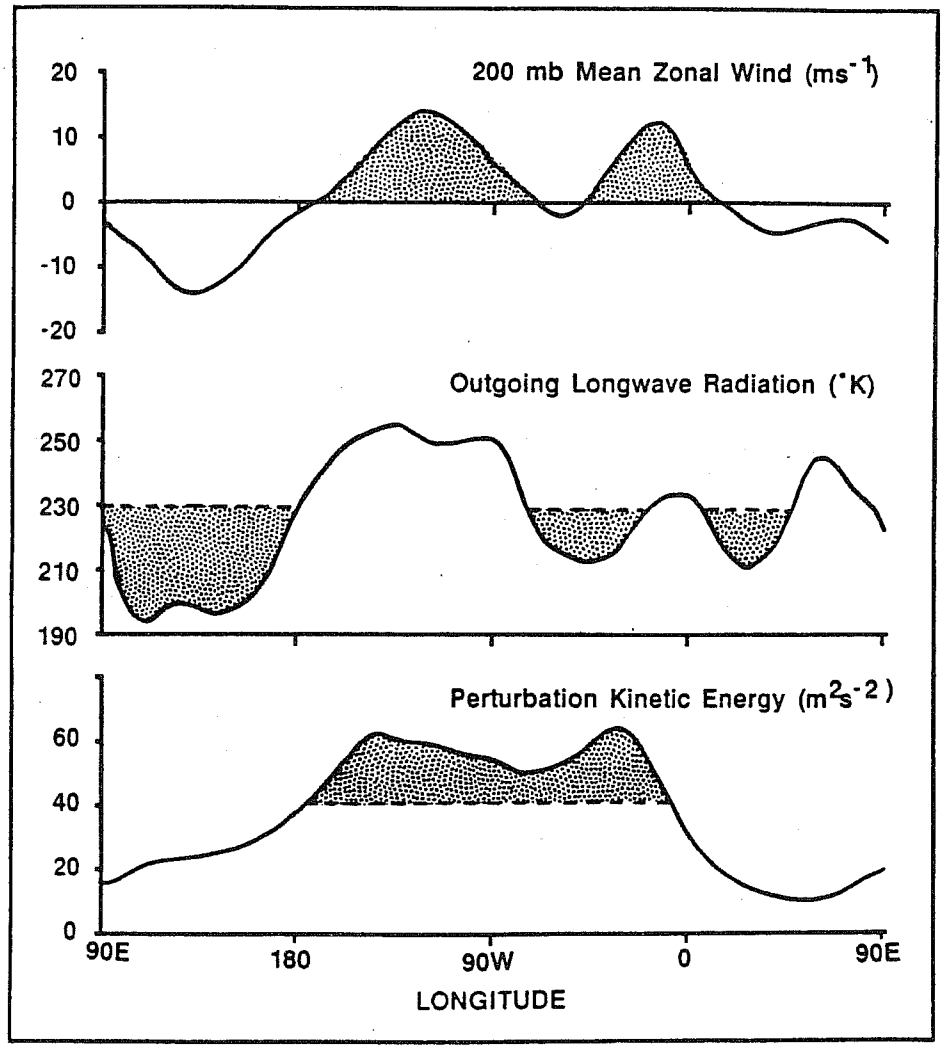

Figure 9: Distribution along the equator of the 200 mb zonal wind (m s^{-1}), the OLR (°K) and the perturbation kinetic energy (PKE; m^2s^{-2}) for the mean boreal winter. Note the strong correlation between westerlies and strong PKE but the association of convection (cold OLR) with the easterly regime. Webster and Chang (1988).

of the equatorial migration of extratropical rotational waves through the regions of upper tropospheric equatorial westerlies which exist within the slowly evolving basic flow. Webster and Holton (1982) developed the theory to explain the large values of PKE existing in the equatorial westerlies and to show the manner in which transients and stationary waves of one hemisphere influence the deep tropics of the other. Although there is some observational evidence for Webster and Holton's westerly duct theory (e.g., Yanai and Lu, 1988), it does not establish a role for the mean convection or transients originating within the convection either in communicating their influence to higher latitudes or in producing the PKE maxima along the equator. Within this model, the tropics are passive, at least locally, and the PKE maxima the result of energy produced outside the tropics

The "Rossby wave train" theory (Opsteegh and van der Dool, 1980; Hoskins and Karoly, 1982; Webster, 1982, 1983) was developed to explain the anomalous perturbation

height fields in the extratropics first noted by **Bjerknes (1969)**. These perturbations appeared to correlate with the anomalous tropical heating occurring during El Niño. This theory postulated that a wave train would emanate from the anomalous heating towards middle latitudes. While there is evidence that a wave train does emanate from the tropics, there is little sign that a wave train actually emanates *directly* from the anomalous heat source. Furthermore, the theory ignores the divergent character of the basic state and the associated equatorial trapping of the response. The theory ignores the transient nature of the convection and does not address the problem of PKE maxima in regions of strong westerlies or of minimum PKE associated with convection. Sardeshmukh and Hoskins (1988) have suggested a modification to the wave train hypothesis. Considering interannual variations, they suggest that nonlinear divergent motions associated with the height source set up a Rossby wave source region in the subtropics immediately poleward of the heating.

The "wave energy accumulation/emanation" theory of Webster and Chang (1988) and Chang and Webster (1990) suggests that the transient disturbances produced by the convection over the warm tropical oceans produced equatorially trapped modes which propagate *along* the equator away from the energy source. The characteristics of these modes are completely governed by the slowly evolving basic state of the tropical atmosphere. Specifically, in the regions of negative stretching deformation (i.e., when $U_x<0$ i.e., to the east of the equatorial westerlies where *PKE* is a maximum), a convergence or accumulation of wave action flux occurs. The regions of wave energy accumulation were also shown to be regions of emanation for transient Rossby wave trains to the extratropics. These equatorial modes possess the same low frequency character as the modes in the accumulation region. Thus, the impact of the high frequency transient forcing in the convective regions is to produce a response at an apparently lower frequency than the forcing in regions where $U_x<0$, and an equivalently low frequency wave train to high latitudes. Chang and Webster (1990) refer to the accumulation and emanation of the transient equatorial modes as "fast teleconnections". "Slow" teleconnection patterns, on the other hand, are the patterns which are associated with the difference fields between climatic epochs such as El Niño and La Niña. The latter teleconnection probably has more to do with the original wave train hypothesis or the modified theory of Sardeshmukh and Hoskins (1988).[4]

The appeal of the accumulation/emanation theory is that it incorporates a role for the transient modes produced through hydrological processes in the warm sea surface temperature regions and allows for a wave train response but from a particular zone in the tropics. The transient response at high latitudes is phase locked. The phase locking, though, is not

[4] A more detailed description of the dynamics of tropical low frequency variability is given in a second paper "Low Frequency Variability in the Tropics and Extratropics" which appears in this volume.

with the region of transient forcing but rather with the region of westerlies of the slowly varying background state. Further, the theory suggests a mechanism for the production of the *PKE* maxima and minima which is consistent with the theory of equatorially-trapped modes in a flow with longitudinal stretching deformation (Webster and Chang, 1988). At the same time, the theory is not inconsistent with the westerly duct theory of Webster and Holton (1982) where extratropical influence propagates into the tropics. Clearly, the accumulation/emanation theory, as well as the wave train hypothesis, requires a thorough understanding of the mechanisms that control the diabatic heating in the tropical atmosphere. Such mechanisms are functions of the coupled ocean-atmosphere system and the hydrology cycle which we will explore in subsequent sections.

3. HYDROLOGICAL PROCESSES AND THEIR IMPACT ON OCEAN-ATMOSPHERE INTERACTION

3.1 Cloud and the Total Surface Radiation Flux

The processes that determine the net radiative flux at the surface of the ocean are shown in Fig. 10. Stephens (1978) related cloud emissivity (ϵ) and albedo (a_c) through the liquid water content of the column in the manner shown in the upper panel of Fig. 10. Along the upper scale, clouds characteristic of the different water paths are indicated (Stephens and Webster, 1983). The albedo increases almost linearily with liquid water path whereas the emissivity rapidly approaches unity for quite small values of liquid water content. That is, clouds that are fairly transparent to solar radiation may be black in the infrared. The total emissivity of a column is also a function of the water vapor in the atmospheric column, a point that is particularily relevant to the tropics.

Some consequences of this $\epsilon - a_c$ relationship pertaining to the ocean-atmosphere system may be seen in the bottom two panels of Fig. 10. Consider a cloud within a dry environment. As cloudiness increases, the solar radiation reaching the ocean surface decreases in proportion to the liquid water content of the cloud. Since the cloud increases, the downwelling infrared radiation from the cloud base ($F_c \downarrow$) will also increase, compensating somewhat for the depletion of the magnitude of the solar stream. However, if the cloud exists within a very moist environment such that there is substantial moisture in the boundary layer, $F_c \downarrow$ will be partially absorbed by the moist boundary layer. Especially in the warm ocean regions of the tropics, the ambient moisture distribution may be so large that the boundary layer itself is radiating as a black body and the effective radiating level is therefore below the cloud. As

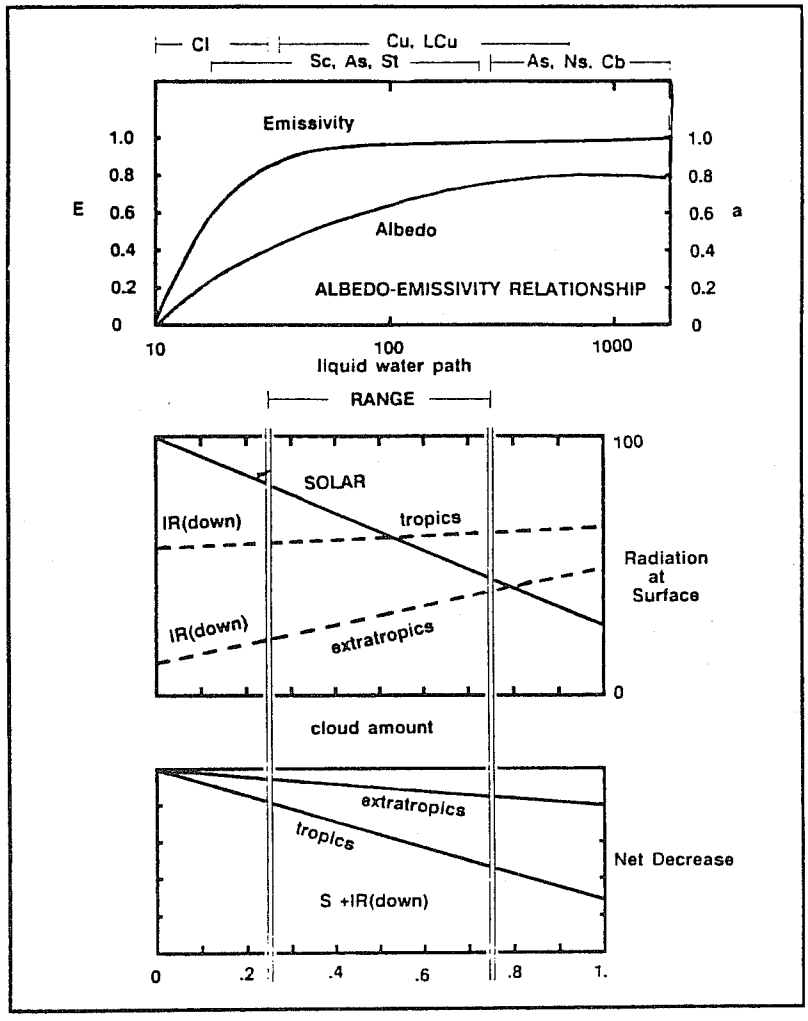

Figure 10: Diagram representing the impact of cloud on the surface radiation budget. Upper panel relates the albedo and emissivity through the liquid water path (Stephens, 1978). The middle panel shows the relative variation of the downwelling IR and solar radiation reaching the surface for the tropics and the extratropics. The bottom panel shows the net percentage irradiance decrease at the surface due to cloudiness for the tropics and the extratropics.

the moisture content of the tropical boundary layer remains much the same between disturbed (i.e., extensive cloudiness) and undisturbed (reduced cloudiness) conditions the atmospheric boundary layer tends to remain optically black at all times. Thus, the impact of clouds in the deep tropics on the downwelling infrared radiation at the surface $F_s\downarrow$ is minimized such that:

$$F_c\downarrow < F_s\downarrow \approx constant. \tag{1}$$

The relative insensitivity of the downwelling infrared radiation to the presence of clouds renders the tropical oceans particularly sensitive to cloudiness variations. The middle panel of Fig. 10 shows the relative decrease of solar and long-wave radiation as a function of cloud amount for the tropics and extratropics as a function of cloud amount. In both

locations, solar radiation will be reduced by roughly the same percentage for the same cloud type if we ignore factors such as differences in cloud composition and solar zenith angles. On the other hand, the downwelling infrared increases only slightly with increasing cloud amount in the tropics but increases substantially at higher latitudes for the reasons discussed above. The bottom panel shows the impact of cloud amount on the net radiation at the surface (i.e., $S_s + F_s \downarrow$). It can be seen that the variation of the solar radiation due to cloudiness becomes the critical factor in the tropics.

It is clear that a detailed climatology of surface solar radiation in the tropics is essential for ocean-atmosphere studies. Additionally, atmospheric models must possess parameterizations that express the real latitudinal and longitudinal variation of the long-wave and short-wave radiative fluxes. This includes, at *all* latitudes, the spatial and temporal variation of $F_c \downarrow$. Even though Fig. 10 indicates that the variation of the downwelling infrared radiation is relatively small in percentage terms (i.e., ±10-15%), the higher values of $F_s \downarrow$ translate to flux variations of between 40-80 W m^{-2} between cloudy and clear regions. In terms of net fluxes at the surface, this is a large number and is four times the measurement goals established for the Tropical Ocean Global Atmosphere Programme (TOGA) for monthly mean quantities. In the next section, we will discuss why it is important that the magnitudes of the components of the surface radiative flux be known quite accurately.

3.2 Impact of Cloud on the Heating Distribution in the Upper Ocean

As discussed in the last section, clouds impact the radiative stream in two ways. Besides varying the magnitude of the total surface radiative flux, $\sum R_s$, clouds change substantially the proportion of long-wave and short-wave at the surface. The total radiative flux may be written as:

$$\sum R_s = S_s - \sum F_s = S_o(1 - a_c)(1 - a_s) + F_s \downarrow - F_s \uparrow, \qquad (2)$$

where S_o and a_s represent the solar constant and the surface albedo, respectively. Over land areas, where short- and long-wave radiation alike is attenuated in the skin layer of the soil or in the biosphere, the heating of the surface is determined by $\sum R_s$ and the fluxes of heat and moisture. In the upper ocean, the situation is very different because the attenuation coefficient of the radiation is a strong function of the wavelength.

Both downwelling long-wave radiation and incoming solar radiation are selectively absorbed in the upper ocean. The absorbtion of solar radiation shows a strong spectral dependence, with the red and near infrared radiation absorbed within a few meters and the shorter wavelength radiation absorbed at considerable greater depths.

Simpson and Dickey (1981) express the intensity of the subsurface solar radiation as an attenuation function, $S_{oce}(z)$, , as:

$$S_{oce}(z) = S_s\left(r\exp\left(\frac{z}{\psi_1}\right) + (1-r)\exp\left(\frac{z}{\psi_2}\right)\right) \tag{3}$$

where r is the proportion following the "red" absorption characteristics with attenuation depth of ψ_1 and *(1-r)* is the proportion in the blue-green end to the "red" end of the spectrum (ψ_2). ψ_1, ψ_2 and r are also strong functions of turbidity, which partly depends on S_{oce} through the stimulation of biospheric activity. Table 1 summarizes the relative absorption of radiation as a function of depth and wavelength. The red end of the spectrum (λ>0.9μ) accounts for about 40% of the incoming beam. The red spectrum has an e-folding depth of about one centimeter. The visible "blue-green" end of the spectrum (λ<0.9μ) represents about 60% of the incoming radiation and attenuates within 8 m of the surface.

Table 1: Energy distribution with depth of the incoming solar beam displayed as a function of wavelength. An incident solar intensity of 1000 is assumed. The spectral dependency of absorbtion falls into two categories which are termed "blue-green" and "red" bands. The percent absorbtion of the total beam and the "blue-green" and "red" is shown together with the e-folding depths of the stream s.

Wavelength (μ)	**Depth (m)**									**proportion**
	0	**10^{-5}**	**10^{-4}**	**10^{-3}**	**10^{-2}**	**10^{-1}**	**1**	**10**	**100**	
0.2—0.6	237	237	237	237	236	229	207	172	14	"blue-green" 59.7%
0.6—0.9	360	360	360	359	353	305	129	9		
0.9—1.2	179	179	178	172	123	8				"red" 40.1%
1.2—1.5	87	86	82	63	17					
1.5—1.8	80	78	64	27						
1.8—2.1	25	23	11							
2.1—2.4	25	24	19							
2.4—2.7	7	6	2							
Sum	1000	993	953	858	729	542	336	181	14	
% Absorbed	0	.7	4.7	14.2	27.1	45.8	66.4	81.9	98.6	
% blue-green	0	0	0	.2	1.3	10.6	43.7	69.6	97.7	e-fold 8m
%red	0	1.3	11.5	34.4	64.8	98.5	100	100	100	e-fold $8x10^{-3}$m

Figure 11 shows the attenuation of incoming solar radiation as a function of wavelength and depth in meters. The histograms denote the proportion of radiation at different depths in the same wavelength bands listed in Table 1. The histograms, set at various depths in the upper ocean, show clearly the strong spectral dependency of attenuation with depth of the visible radiation. The percentages refer to the amount of solar radiation, integrated over all wavelengths, reaching a particular depth. The downwelling atmospheric infrared radiation

(i.e., $F_s \downarrow$) is attenuated at the same rate as the "red" spectrum described above. Similarly, the infrared emission from the surface (i.e., $F_s \uparrow$) emanates from a very shallow layer.

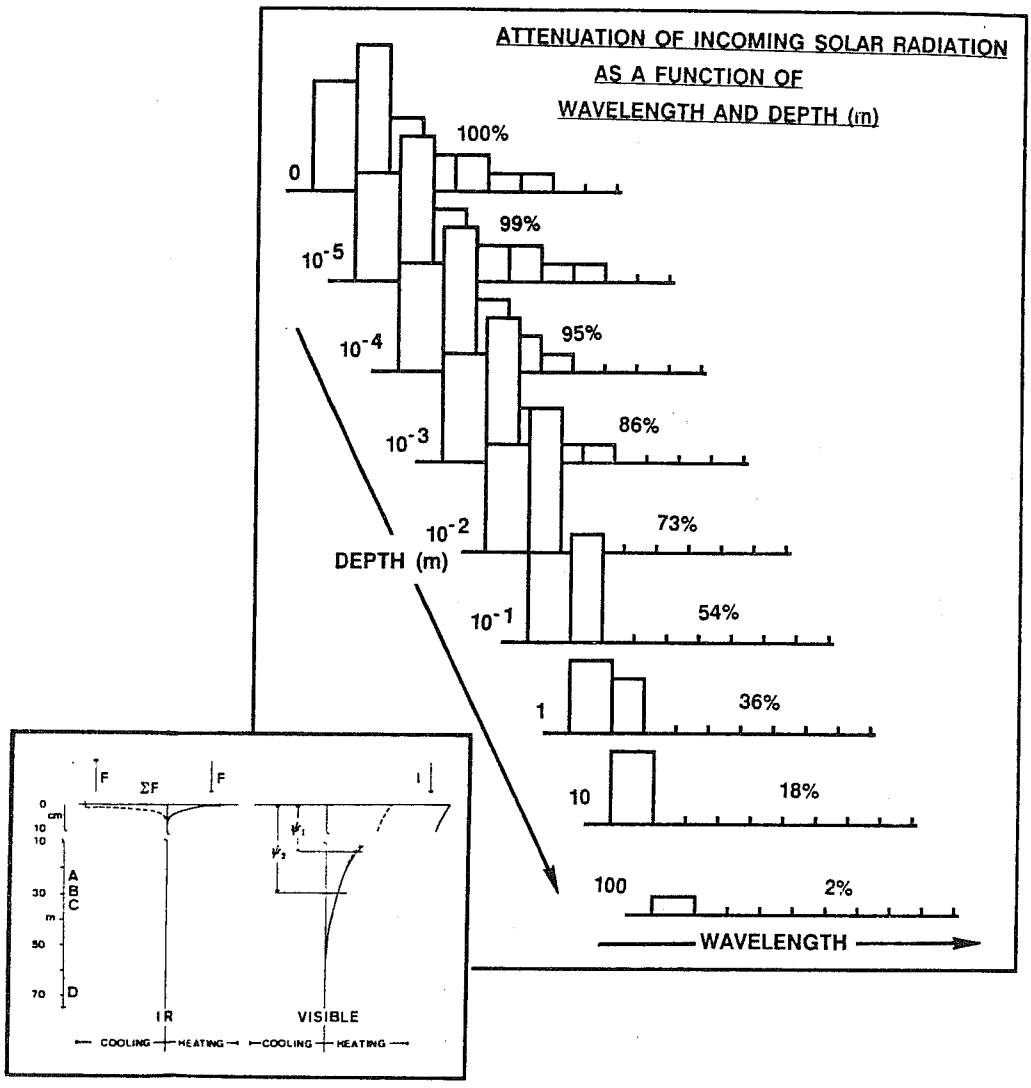

Figure 11: Amplitude variation of the solar spectra as a function of depth through the upper layers of the ocean. Percentage refers to the amount of the incident solar beam reaching the indicated depths. Inset shows the attenuation of the total irradiance (solar plus IR) as a function of depth. The lettering A,...D refers to mean thermocline depths of various parts of the ocean.

One must be careful in interpreting both Table 1 and Fig. 11. It should be remembered that there is also substantial selective absorption of the incoming solar beam by the ambient water vapor and clouds in the atmosphere. Although subject to reflection by clouds, the blue-green end of the spectrum will be transmitted to a greater degree than the red and near-infrared end of the spectrum. This attenuation of long-wave radiation is accomplished by water vapor in the boundary layer of the tropics and emphasized considerably by clouds during disturbed events. Furthermore, as surface albedo has a strong spectral dependence, surface albedo should also be a function of cloud cover.[5]

5 J. Curry, personal communication.

The insert at the bottom left of Fig. 1 provides another perspective of oceanic attenuation for both the infrared and the visible stream s. As $F_s \uparrow > F_s \downarrow$, the infrared cooling of the ocean takes place in a very shallow layer. However, the solar radiation is spread much deeper through the upper ocean. The depths labelled A, B, C and D show the average thermocline depths for the summer extratropics, the average tropics and the east and west equatorial Pacific Ocean during non-El Niño periods when the SOI ≥ 0. During warm events (SOI << 1), the average thermocline depth is somewhere between C and D. Note now, the importance of the magnitudes of the attenuation depths ψ_1 and ψ_2. If $\psi_2 > z(A, ...D)$ in a particular location, then the slow dynamics of the deeper ocean must compensate for the diurnal heating at depths greater than the thermocline depth, h_c. Woods (1984) contended that during a period of rapid transition in the Pacific from one climate epoch to another, the variation of cloudiness which may accompany the change may produce solar heating below the thermocline in regions where, initially, there was a deep thermocline (i.e., h_c large) and high cloudiness such as in the western Pacific when SOI ≥ 0. Woods felt that this anomalous heating could be significant in a climate sense as it could not be redistributed rapidly by mixed layer dynamics. In summary, if $h_c \gg \psi_2$, then variations in the radiation balance will be constrained to effects within the mixed layer. On the other hand, $h_c \geq \psi_2$, then solar radiation may be absorbed below the thermocline and may be unaffected by the rapid dynamic and thermodynamic adjustments of the mixed layer. Other slower, processes would then be required to disperse the heat accumulations.

3.3 Episodic Heat, Moisture and Momentum Fluxes from the Atmosphere to the Ocean Through Moist Tropical Events

In the Pacific and Atlantic Oceans, the general easterly flow of the trade winds and near-equatorial surface winds produce a wind stress that drives a slope of the surface water upwards from east to west. During ENSO, changes in the coupled system cause the stress to vary successively, producing enhanced slope during the La Niña phase (i.e., SOI >> 0) and reduced slope during El Niño. Commensurate with the changes in surface height distribution are variations in the heat content of the upper ocean and alterations in the distribution of SST. However, throughout the very low frequency evolution of ENSO, the system is subject to strong higher frequency local stochastic forcing associated with episodic convection. During these episodes, a series of moist convective events transfer large amounts of momentum into the ocean as well as introduce large amounts of fresh water. Disturbances often appear in groups which render the western Pacific to a state of intense

convective activity for a prolonged period. The disturbed period is often associated with strong surface westerlies, often called a "westerly burst". Figure 12 (from Nakazawa, 1988) shows the broad-scale convection, the detailed convection and the wind fields associated with a westerly burst. Within an envelope of macroscale organized eastward propagating convection, a series of synoptic disturbances counter-propagate towards the west.[6] To the east and west of the disturbances are lower tropospheric easterlies and westerlies. The stronger westerlies are the westerly burst.

The combined momentum fluxes from the disturbances and the burst have been observed to produce a significant oceanic response in the form of an eastward propagating Kelvin wave (Knox and Halpern, 1982, Luther, Harrison and Knox, 1983). Following a burst near 175°E during April, an oceanic Kelvin wave migrated eastward. Figure 13 shows the variation of the wind at Ocean Island in the western Pacific and the variation of the eastward transport per unit width of the mean zonal current averaged between the surface and 250 m along the equator at 152°W and 110°W and by the sea level variation at Isabela Island in the Galapagos (Knox and Halpern, 1982). The ocean signal arrived at the three stations on April 7, April 25 and May 3, respectively, indicating phase speeds between each station pair of about 2.7 m s^{-1}. Thus, episodic variations in the west associated with convection appear to cause substantial remote effects (i.e., oceanic teleconnections) in the ocean.

Although something is known about the frequency and spatial and temporal variability of climate epochs such as El Niño (see Philander, **1989**), little is known about the genesis or form of the westerly bursts which evolve very rapidly over scales of thousands of kilometers along the equator. There is some evidence that the bursts originate as incursions into the tropics during cold surge events (Williams 1981; Webster, 1987; Love, 1985), although it may be that the bursts develop *in situ* through some form of instability probably strongly associated with the hydrology cycle.

Figures 14(a) and (b) show latitude-longitude maps at 850 mb and vertical cross-sections along 5°S during an intense westerly burst in January, 1979. The burst lasted nearly a month, compared to the week to two week period that is closer to the norm. To indicate the length of the burst, 850 mb winds plotted over a six month period are shown in Fig. 14(c) for indicated times and locations. Whereas the January burst was unusual for its duration, it is typical of bursts in terms of its longitudinal (> 5000 km) and latitudinal scale ($\approx$ 15°). Maximum winds occurred along 5°S. Height sections along 5°S show that

[6] There are two theories which explain the rapidly propagating westward modes moving eastward within a slow eastward moving envelope. The first (Lau, *et al*, 1990) considers the envelope to be a slowly moving viscous Kelvin wave and the westwards as modes shedded Rossby waves. The second theory considers the envelope to be the group of sets of eastward propagating Rossby modes. In fact, using calculations by Webster and Chang (1988), the magnitudes of the eastward group velocity and westward phase speeds are about correct to explain the phenomena.

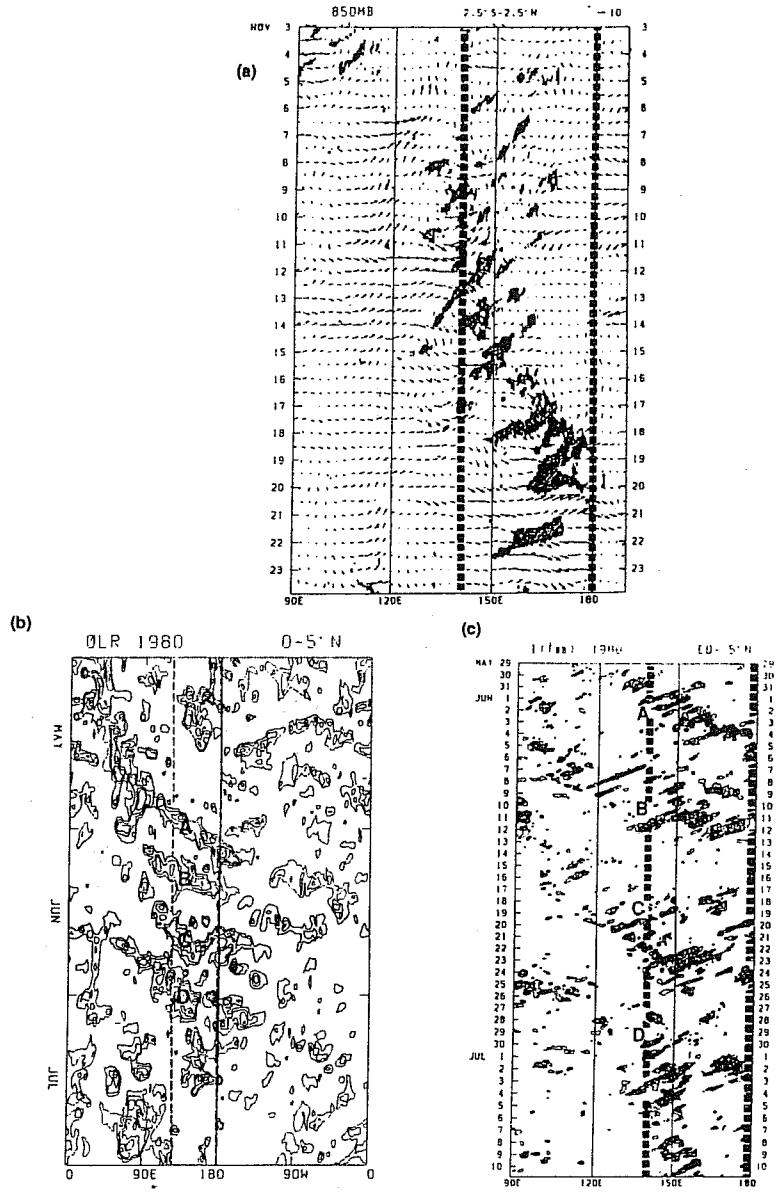

Figure 12: (a) Time-longitude section of the OLR averaged between the equator and 5°N from May through June, 1980 with the seasonal trend removed. Contour interval is 30 W m^{-2} with a threshold of –15 W m^{-2}. Lettering denotes "super-clusters". (b) Same as (a) but just over the western Pacific Ocean. To highlight the deepest convection only the "coldest" emission is shown. Lettering corresponds to lettering in (a). Super clusters propagate to the east but higher frequency components propagate to the west through the "slow envelope". (c) 850 mb zonal wind field (m s^{-1}) along the equator for the same time period. Solid curves denote westerlies. Calculated from the ECMWF data set. Panels (a) and (b) are from Nakazawa (1988).

the westerlies extend at least through the mid-troposphere and eventually encroach into the upper troposphere. Again, the January, 1979 case is somewhat different as generally the westerlies are restricted to the lower troposphere with strong easterlies aloft.

Case studies of westerly bursts by Ramage and colleagues (private communication) indicate a clear association between the bursts and strong convection, consistent with the findings of Williams (1981). The observations suggested a sequence in which an initial westerly wind along the equator was followed by an intense development of organized convection. With this development, the westerly winds accelerate along the equator. Often

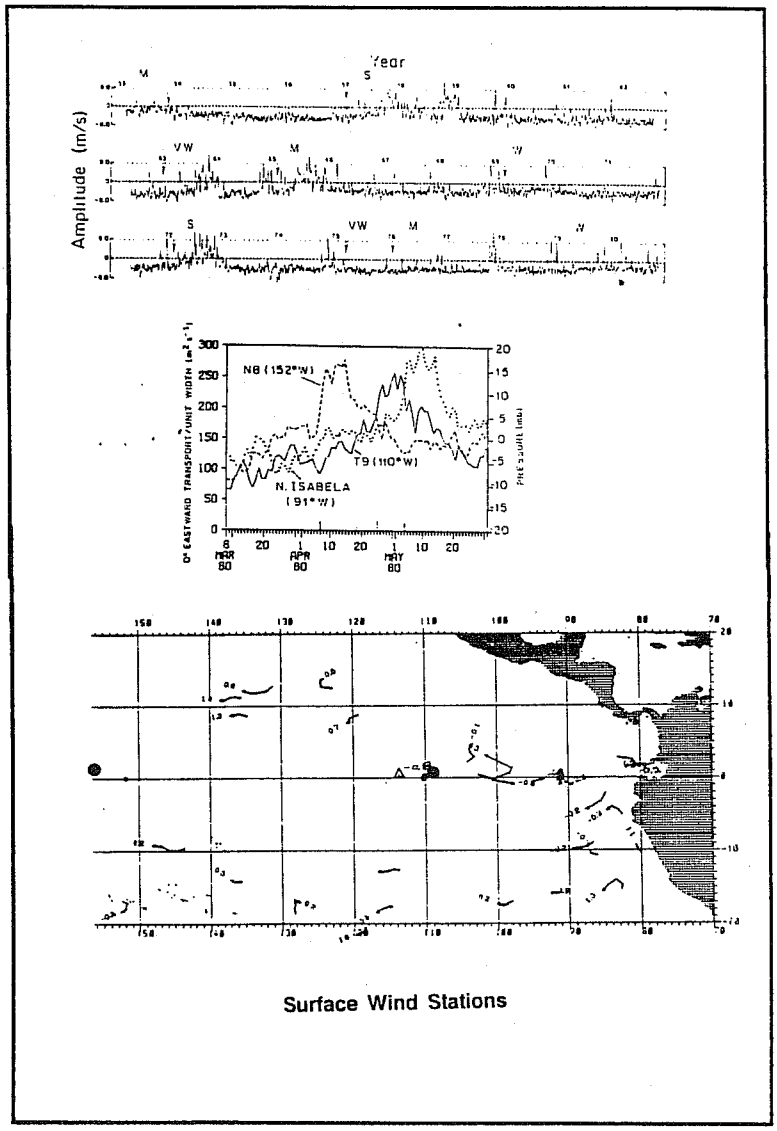

Figure 13: Surface wind speed variation at Ocean Island (170°E) along the equator. The second panel shows the variation of mixed layer characteristics along the equator at the locations indicated in the lower panel following a westerly "burst" in the western Pacific in April, 1980. Observations suggest that the burst initiated a Kelvin wave that propagated eastwards at a speed of 2.7 m^{-1}. (Knox and Halpern, 1982; Luther, Harrison and Knox, 1983).

the acceleration was followed by the formation of dual cyclone pairs on either side of the equator at which time the convection on the equator subsided. The westerly winds, however, were then sustained for an even longer period by developing cyclone pairs. Lukas (1988) has suggested that successive westerly bursts are of primary importance in the longer period ENSO cycle. We will discuss this hypothesis in conjunction with the impact of a fresh water flux into the ocean in the next section.

3.4 Precipitation and Fresh Water Input Into the Ocean

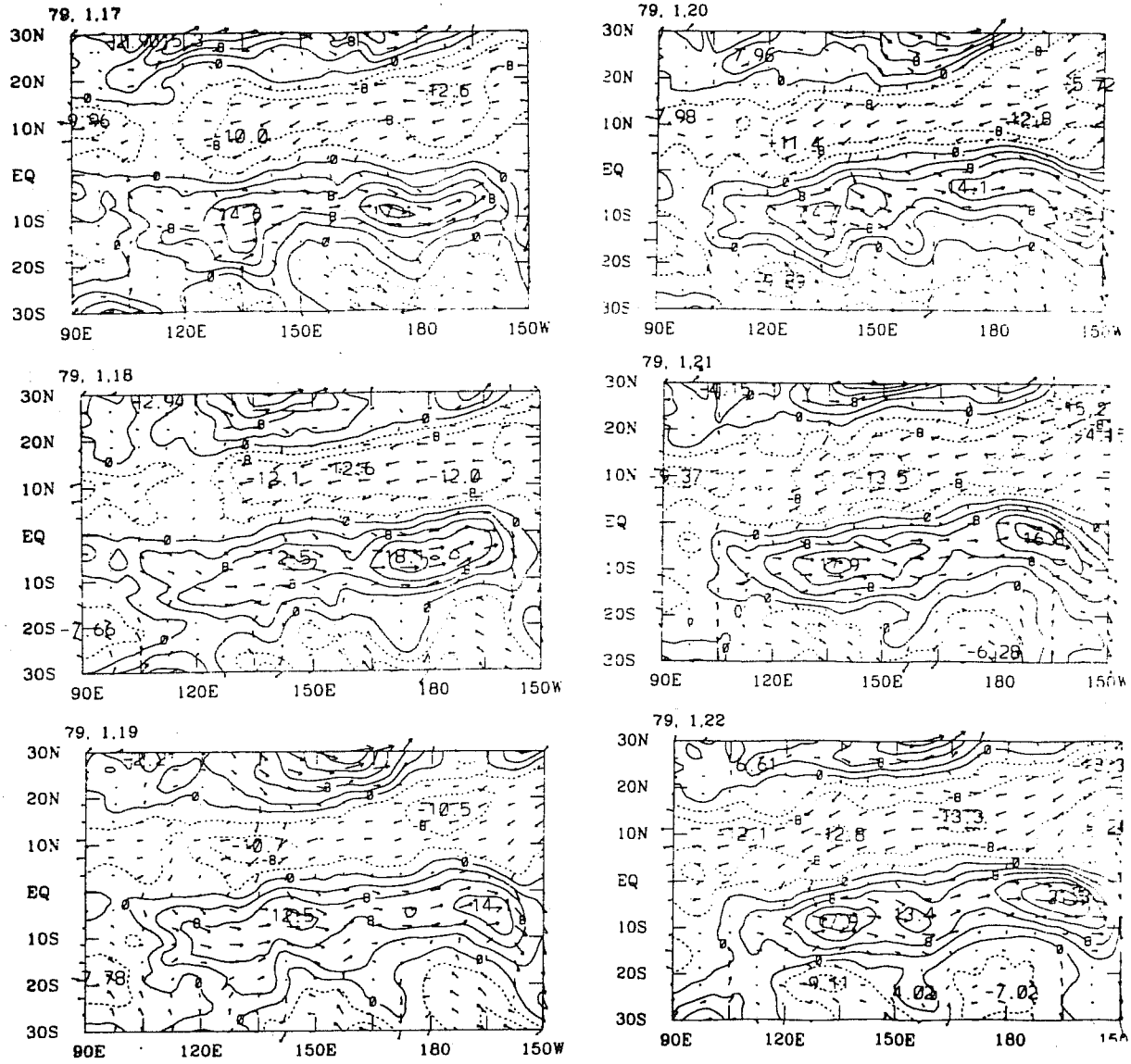

Figure 14(a): The 850 mb wind field for six days in January, 1979. An intense westerly burst maintained its position between 120°E and 150°W for almost a month. Maximum winds in excess of 20 m s^{-1} were located off the equator at about 5°S. Climatological values show very weak westerlies to the west of the dateline. Data from ECMWF.

In previous paragraphs we have mainly addressed the direct influence of the hydrology cycle on the temperature of the upper ocean. However, in addition to the momentum flux from the atmosphere to the ocean and the variation of the radiational heating due to cloudiness effects, body forces may arise from salinity gradients in the upper ocean. From (5) we see that the density of the ocean is a function of temperature and salinity so that body forces may arise from variations in either or both quantities. Equation (7) indicates that a number of factors vary the buoyancy of a column. In the ocean, salinity varies as a function of the fresh water input from precipitation, from fresh water loss due to evaporation (i.e., collectively as *P-E*), and by advection of anomalously saline water from other regions

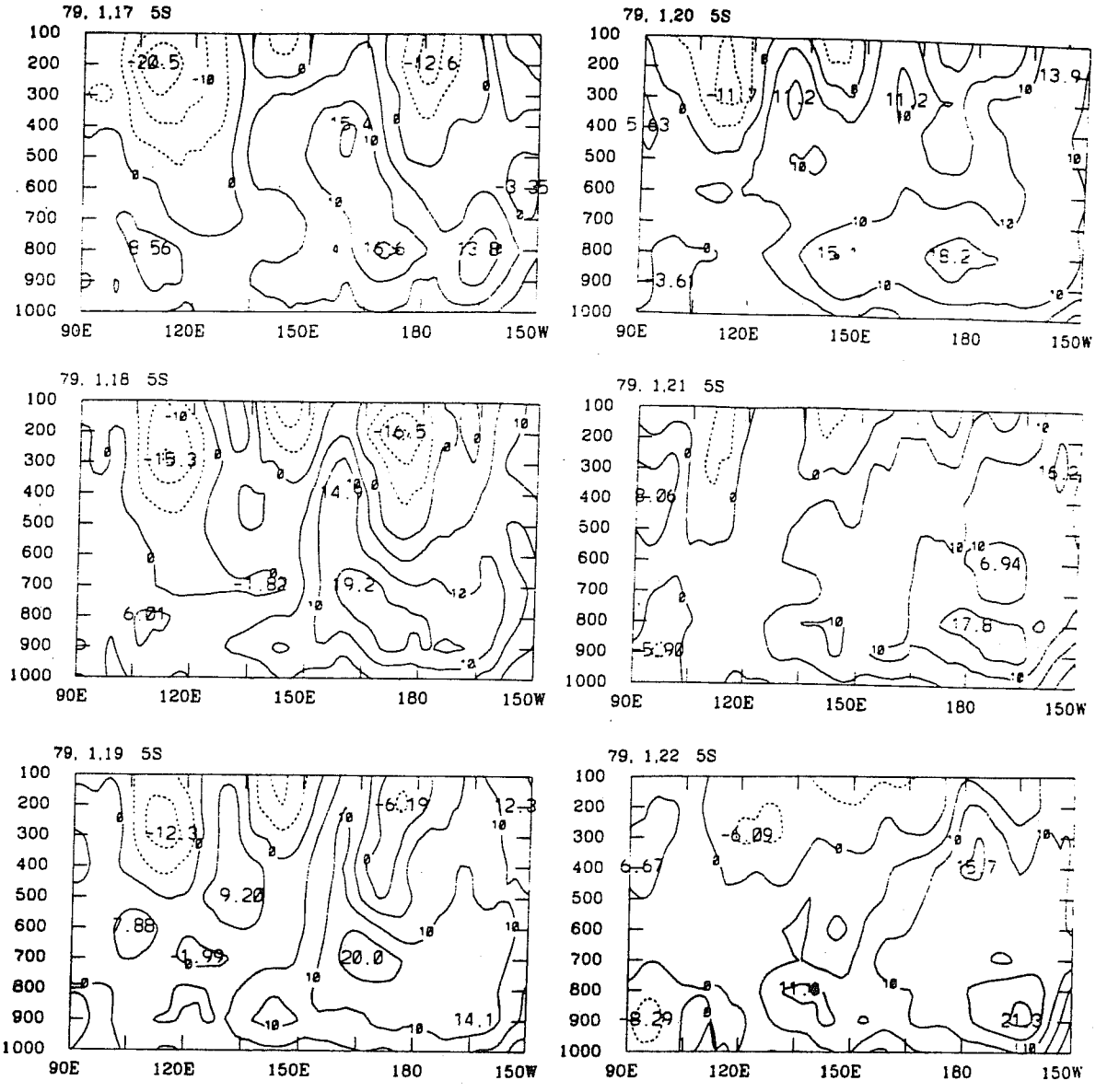

Figure 14(b): Cross section of the zonal wind component along the equator from 0°E to 160°W. This particular burst was unusual in that westerlies eventually extended throughout the troposphere. More often, the strong westerlies in the lower troposphere are coupled to anomalously strong easterlies in the upper troposphere. Data from ECMWF.

or depths and by river inflow. In the western and central Pacific Ocean, probably all of these processes are important. The first two (precipitation and evaporation) are integral parts of the hydrology cycle. The third, advection, may be partly a response to the body forces modified by the hydrology cycle.

How important are these fluxes of fresh water? Godfrey **(1990)** has made a careful estimate of the various contributions to the buoyancy flux in the warm pool regions of

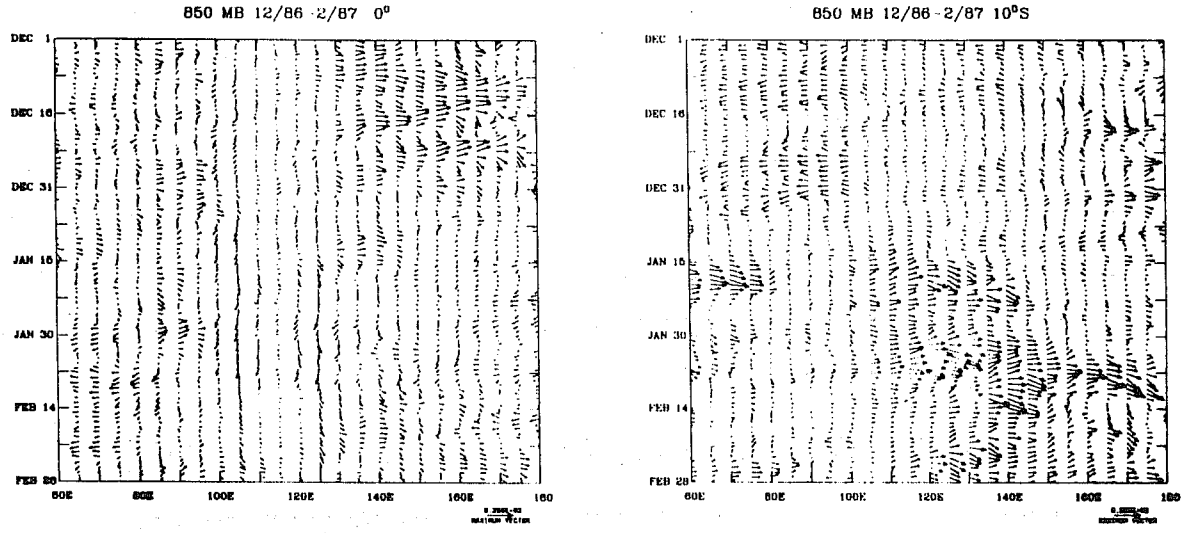

Figure 14(c): Time sections along the equator and 10° S for the period December 1, 1986 through February, 1987 which covered the AMEX/EMEX period. A series of strong westerly bursts may be seen in early December along the equator. However, strong westerlies did not occur further south until January with the onset of the Australian monsoon. Note, though, that the monsoon westerlies extended to at least the dateline, some 4000 km east of Australia. Data from ECMWF.

the tropical oceans.[7] Godfrey concentrated on the western Pacific Ocean because of the sensitivity of its character to changes in its buoyancy flux and the sensitivity of the overlying atmosphere to small changes in the boundary forcing. Using Oberhuber's (1988) estimate of the (P-E) of about 2 m, Godfrey estimated that the buoyancy flux due to fresh water flux is about 4–6 cm/year.[8] On the other hand, if it is assumed that the net heat flux is of order 20 W m^{-2}, then the modified buoyancy flux due to the surface heat flux is also about 4 cm/year! That is, salinity variations in the upper ocean are probably just as important as temperature variations. In fact, Lukas **(1988)**, using WEPOCS data gathered in the western Pacific, has shown that the depth of the mixed layer, defined by density discontinuity as in Section 3.2(ii), is determined by salinity as often as by temperature.

It is possible to form a conceptual model that satisfies the observations and that would be tested through modeling or ancillary observations. Westerly winds in general, from whereever they arise, are convergent towards the equator and thus, equatorially trapped. Consequently, the westward flow must be associated with moisture convergence and thus, with convective development. Equatorial westerly winds are also consistent with downwelling in the ocean so that the sea surface temperatures may be expected to remain warm and supportive of organized convection. Furthermore, the input of fresh water from

7 Also published in the minutes of the Eighth TOGA Scientific Steering Group, Hamburg, September, 1989.

8 Godfrey defined buoyancy flux slightly differently to our definition in (7) by dividing by g. Although his "buoyancy flux" does not now have the correct units, its allows a very direct, and rather meaningful, comparison with other quantities. As the modified B has units of m s^{-1}, the impacts of heat flux and fresh water flux can be thought of as a change in steric height (assuming advective effects do not remove the more buoyant layer) and be compared to wind induced surface elevation changes.

convection (to be discussed in detail in the next section) will stabilize the mixed layer and reduce the mixing up of the colder water. At the same time, the stable fresh layer, insulated from the cooler water below, will heat due to the trapping of solar radiation. Perhaps the already warm water, warmed further in the thin, stable layer, enters into a positive feedback mechanism not unlike convective instability of the second kind. Thus, initial westerlies along the equator and the resulting convergence and precipitation will produce stronger westerlies, and so on. The constraining mechanism may be the stronger mixing caused by the resultant westerly burst which accesses the cooler deeper water. A schematic diagram of the sequence is shown in Fig. 15.

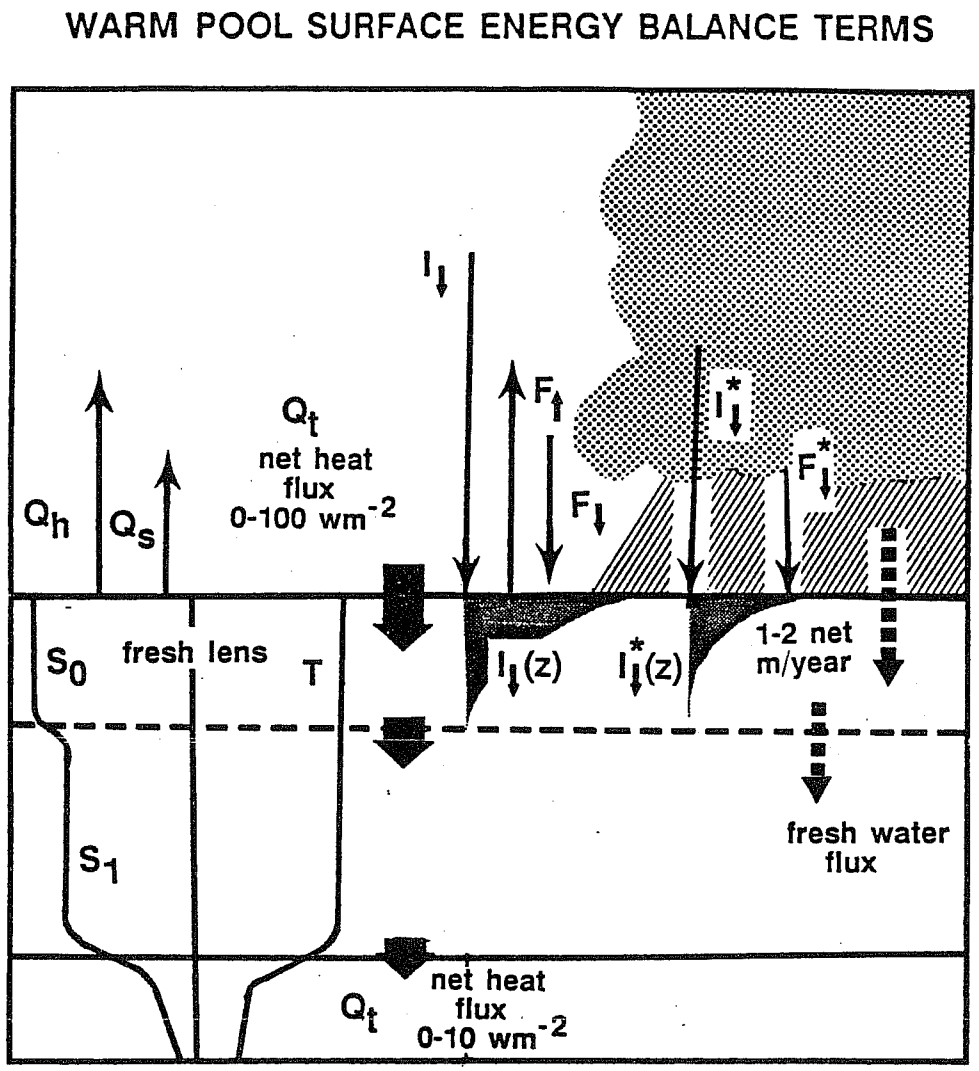

Figure 15(a): Energy balance of the tropical warm pools. Surface fluxes of momentum, fresh water, latent heat and radiation are affected considerably by the hydrology cycle. The short-wave flux, I, is affected especially. The fresh water flux, positive into the ocean, creates the fresh lens which will be evident until anomalously strong momentum fluxes occur.

3.5 Clouds and Total Diabatic Heating in the Ocean-Atmosphere System

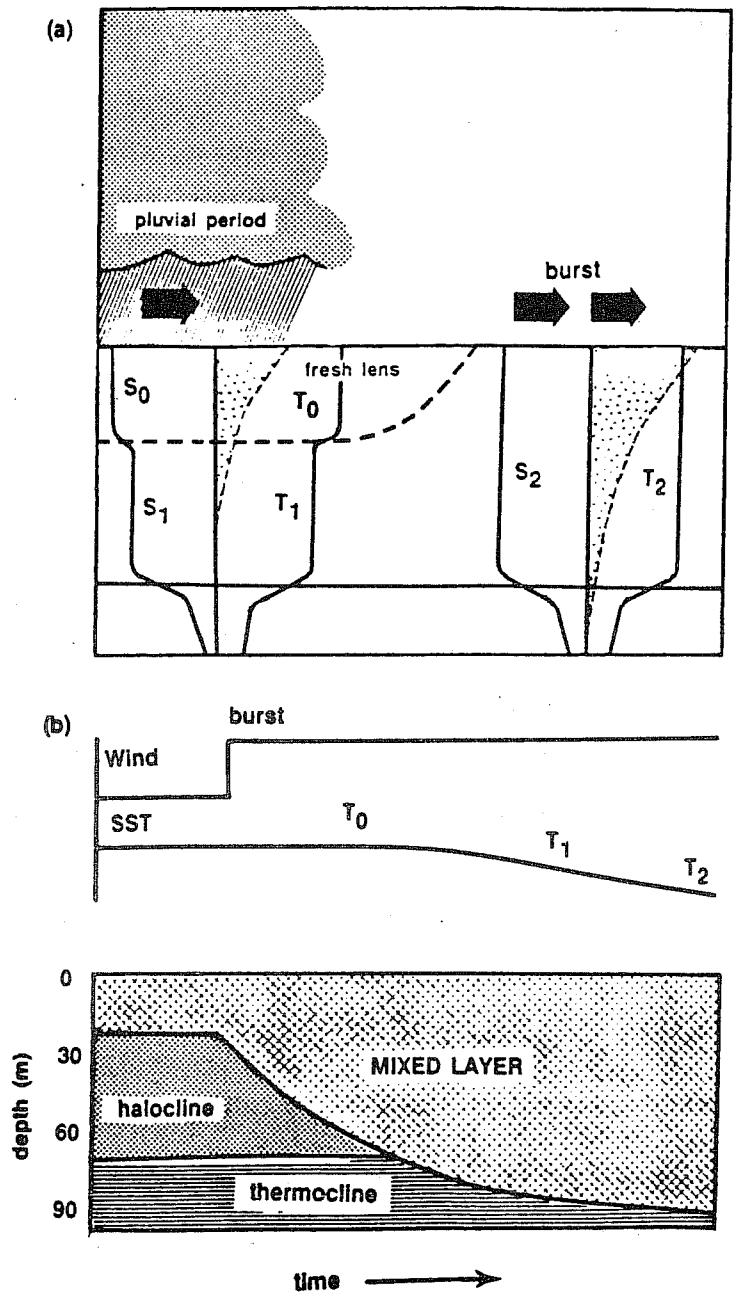

Figure 15(b): Schematic sequence of events in the warm pool region of the tropical Pacific. Pluvial period produces a fresh lens which stabilizes the upper ocean. Solar heating anomalously warms surface layer which, in turn, enhances broad scale convective activity which may produce a westerly burst. If the burst is sufficiently strong, as indicated in the bottom panel, cool saline water will be accessed from below the thermocline and the upper ocean will cool. Lukas and Lindstrom (1987).

In the Introduction we indicated that the gradients of radiative flux convergence in the troposphere (ΔQ_{rad}) was a substantial fraction of the latent gradient (ΔQ_{lh}) and of the same sign. We will now compute an order of magnitude estimate of the two gradients. Further, we will assess the importance of the decreased heating in the ocean column consistent with the atmospheric radiative structure and compare the sign of the resultant gradient with the atmospheric heating gradients.

Consider a very simple atmosphere represented by four columns, *I*=*A, B, C* and *D*, representative of the desert regions of North Africa, the monsoon region of South Asia and the western and eastern Pacific Ocean. The surface temperature of the columns are $T_s(I)$, where *I*= *A,..,D*. The cloudy region is assumed to be sufficiently thick so that the cloud radiates to space at the cloud top temperature $T_t(I)$ and towards the ocean surface at the temperature of the cloud base $T_b(I)$. The boundary layer below the cloud is assumed to be moist with an emissivity $\epsilon_{bl}(I)$ so that partial absorption of the downwelling longwave flux from the cloud occurs in the boundary layer. The temperature of the boundary layer is set at $T_{bl}(I)$.

In a very cloudy region, where the cloud emissivity is assumed to be in unity, an expression for the radiative flux convergence ($Q_{rad}(I)$) in the column *A* is:

$$\{Q_{rad} = S_0(1-\alpha_c) + \sigma T_s^4 - (1-\epsilon_{bl})\sigma T_b^4 - \epsilon_b \sigma T_{bl}^4 - \sigma T_t^4\}_I. \quad (4)$$

In cloudless or moderately cloudy regions where we can assume that the cloud emissivity is less than unity (i.e., $\epsilon_a < 1$), the radiative flux convergence may be expressed as:
Using the data from Table 2 we can calculate the gradients of latent and radiational heating between the various columns. Within the confines of this very simple model, we find that the gradient of the radiative flux convergence across the Pacific Ocean associated with the cloudiness variations is within a factor of three of the latent heating gradient, which parallels the estimate of Ramanathan (1987). Furthermore, significant gradients exist between the South Asian region and the North African deserts with magnitudes that parallel the latitudinal gradient across the equator. Thus, once the monsoon is established, strong gradients are set up in the lateral direction in addition to the longitudinal gradient.[9] Figure 16 summarizes the results of the calculations by showing the heating longitudinal and latitudinal heating gradients between the locations listed in Table 2. Of course, better models may give more accurate comparisons between the two gradients. The simple model used here was constructed merely to provide an order of magnitude estimate. However, it is unlikely that the model gives errors beyond factors of two. In other words, forcing due to the presence of clouds cannot be neglected.

$$\{Q_{rad} = S_0\alpha_c + \epsilon_a \sigma T_s^4 - 2\epsilon_a \sigma T_a^4\}_I. \quad (5)$$

[9] Yang and Webster (1990) have shown that the lateral gradient is of the same magnitude as the longitudinal gradient and is responsible for considerable interannual variability of the monsoon flow. Although the east-west gradient does not possess a significant magnitude until convection commences in South Asia, variations in the radiational cooling over the North African deserts introduce considerable variability into the monsoon. The east-west heating gradient provides lateral linkages between the monsoon and other regions beyond the "traditional" continental-ocean connection.

Table 2: Values of definitely parameters for the four columns (A, B, C and D) of Fig. 19 which represent North Africa, South Asia, South Indian Ocean and the East Pacific Ocean. Lower rows show differences of the latent, radiative and total heating between the columns calculated from (10) and (11). Conditions are for the boreal summer.

Quantity		Columns			
		A	B	C	D
Surface Temp. (°K)	T_s	308	303	298	298
Cloud Base Temp. (°K)	T_{cb}		285	285	285
Boundary Layer Temp.	T_{bl}	300	298	289	289
Cloud Top Temp. (°K)	T_{ct}		220	265	265
Mean Atmos. Temp. (°K)	T_a	275	275	270	270
Cloud Albedo	α_c		0.3	0.2	0.15
Absorbtion Coeff.	a		0.15	0.1	0.1
Emissivity	ϵ	0.6	1.0	0.6	0.6
Emissivity (bl)	ϵ_{bl}	0.6	1.0	0.8	0.7
Precip. Rate (mm/day)	r	0	10	3	2
Latent Heating (wm^{-2})	Q_L	0	289	82	58
Radiative Heating (wm^{-2})	Q_R	-83	59	-41	-56

$$\Delta Q_L(A \rightarrow B) = 289;\ \Delta Q_R(A \rightarrow B) = 142;\ \Delta Q(A \rightarrow B) = 431$$

$$\Delta Q_L(B \rightarrow C) = 207;\ \Delta Q_R(B \rightarrow C) = 100;\ \Delta Q(B \rightarrow C) = 307$$

$$\Delta Q_L(B \rightarrow D) = 231;\ \Delta Q_R(B \rightarrow D) = 115;\ \Delta Q(B \rightarrow D) = 346$$

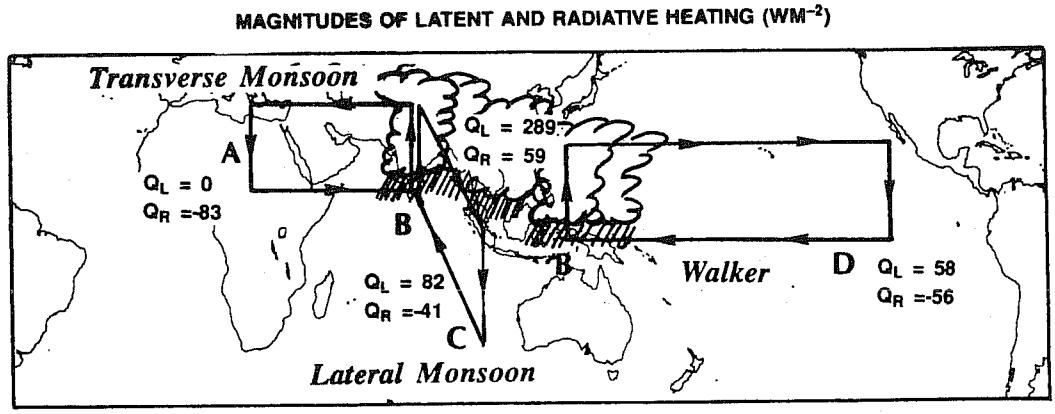

Figure 16: Schematic diagram showing the latent and radiative heating in columns associated with the Walker Circulation and the lateral and transverse monsoon cells. Yang and Webster (1990).

We note, once again, that the latent heating and radiative gradients *will always be of the same sign.* That is, when the dynamics of the atmosphere-ocean coupled system conspire to

provide moisture convergence and ascent and, thus, establish the gradient of latent heating and cloud mass, a corresponding radiative heating gradient will be set up sequentially. In a sense, the radiative heating locks in the latent heating gradient through positive feedback.

The depletion of the solar radiation below the cloudy regions was discussed in Sections 3.1 and 3.2. It is a simple matter to calculate the upper ocean heating gradient between the cloudy and the clear regions. For example, Ramanathan (1987) estimates that the gradient is about 1 to 1.5°C/month averaged over a 100 m layer of the ocean. The interesting fact is that the heating gradient is in the opposite sense to the radiational and latent heating gradient in the atmosphere! That is, anomalous radiative flux convergence in the atmosphere is accompanied by a reduced solar flux at the surface of the ocean. Thus, radiative heating in the atmosphere is countered by anomalous cooling of the oceans or a reduction in the buoyancy flux into the upper ocean. Figure 17 shows a schematic representation of the heating gradients within the coupled ocean-atmosphere system.

3.6 Modeling the response of the upper ocean

To assess the impact of variations in the radiative heating on the upper ocean, we utilize Garwood's one-dimensional ocean mixed layer model (Garwood, 1977 and Garwood *et al*, 1985). The simplicity of the model allows us to conduct sensitivity tests with respect to heat, fresh water and momentum fluxes and to modifications to the radiation schemes. At the same time, a one-dimensional model does not allow the calculation of the lateral response of the model to changes in the buoyancy flux, and, consequently, the horizontal density gradient. Surface and sensible heat fluxes are determined using bulk aerodynamic methods.

Figure 18 shows a schematic diagram of the model mixed layer of depth h which is defined in terms of density. The configuration of the model used contains 200 one-meter levels and is both salt and temperature stratified. Thus, the density structure, and hence, the mixed layer depth, can be produced by discontinuities in either salinity or temperature. The initial conditions of the model were set up in the following manner. An initial surface temperature, T_0 is defined which is assumed to decrease with depth at a rate of $4\text{x}10^{-3}$K m^{-1}. A constant salinity of $S_l = 34^0/_{00}$ is assumed in the initial instance through the entire column. Buoyancy is defined as:

$$B = \alpha T - \beta S_l \tag{6}$$

where S_l represents salinity. α and β are the thermal and salinity expansion coefficients, respectively, and are defined as:

$$\alpha = -\frac{1}{\rho_0}\frac{\partial \rho}{\partial T} \; ; \; \beta = \frac{1}{\rho_0}\frac{\partial \rho}{\partial S_l}. \tag{7}$$

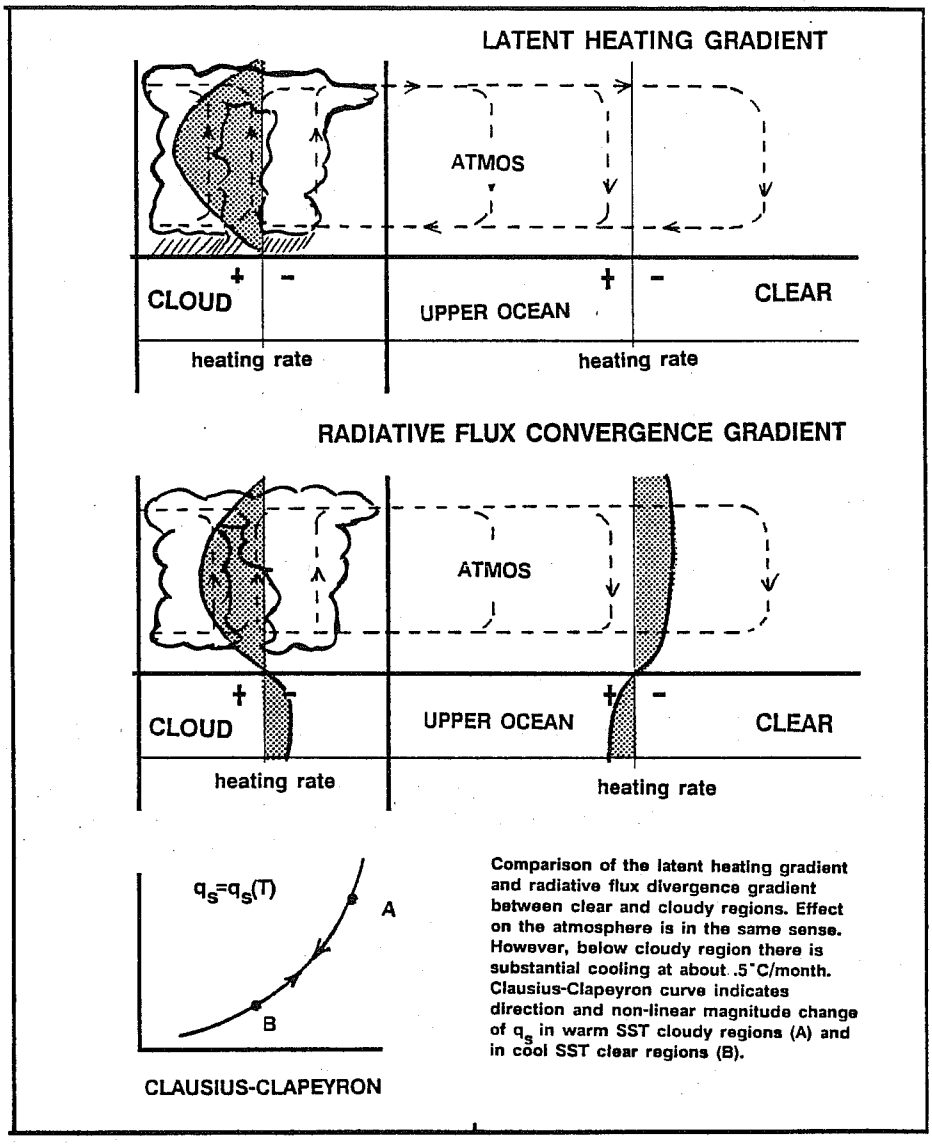

Figure 17: Comparison of the latent heating gradient and the radiative flux divergence between the west and east Pacific (SOI < 0). In the atmosphere, the latent heating gradient is enhanced by the radiative effects. However, in the ocean, the region below the cloud is cooled relative to the clear region. Differential heating of the upper ocean has been estimated by Ramanathan (1987) to be about 1°C/month averaged over a 100 m depth. Clausius-Clapeyron curves indicate the significance of cooling the ocean below the convective regions.

Fresh water flux (i.e., P-E) and heating fluxes H (latent, sensible and radiational) in the upper layers and throughout the column alter the structure of the column by collectively providing a buoyance flux is given by:

$$B_f = \beta g S_l (P - E) + \alpha g H. \tag{8}$$

Thus, if there is a positive buoyancy flux into the ocean (such as will occur if (P-E)>0 or H>0), the density of the upper layer will decrease and the mixed layer will become shallower. If mixing takes place, either by wind stress or by gravitational instability induced by cooling at the upper surface, the ocean column will tend to become homogenized and a new, deeper mixed layer will be formed.

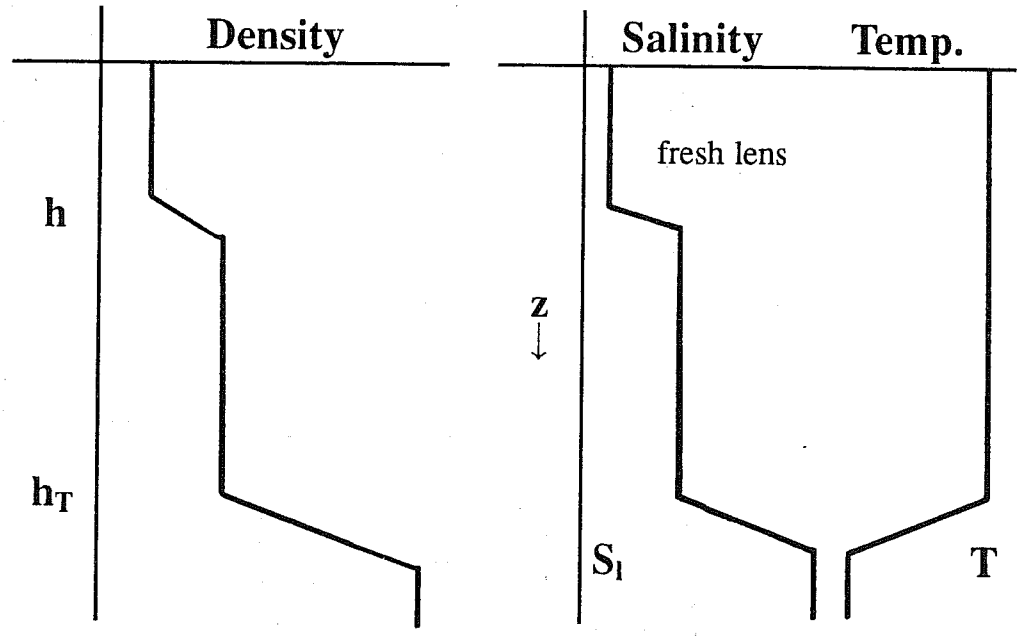

STRUCTURE OF THE GARWOOD MODEL

Figure 18: Schematic diagram of the upper ocean structure of the Garwood mixed layer model. The figure depicts a mixed layer of depth h which is defined in terms of salinity and temperature. The curves to the right show profiles of temperature and salinity typical of the western Pacific Ocean (Lukas, 1987) and consistent with the density profile shown. Note that the density defined mixed layer depth (h) of Garwood is very different than the temperature based definition (h_T) of Kraus and Turner (1967).

The downwelling solar radiation is defined by

$$S = S_0(1 - \alpha_s)T(l)\cos\zeta \tag{9}$$

where $T(l)$ is the solar tranmissivity which is a function of the vertical liquid water path l of a cloud. The solar zenith angle, ζ, is defined as:

$$\cos\zeta = \sin\phi\sin\delta + \cos\phi\sin\delta\cos h_0 = \mu \tag{10}$$

where ϕ, δ and h_0 represent the local latitude, the solar declination angle, and the local hour angle of the sun (Sellers, 1972). The e-folding attenuation depth of solar radiation is assumed to be 10 m unless stated otherwise. Furthermore, for simplicity it will be assumed that the net heat flux away from the ocean surface is a constant. To incorporate more adequately variations in cloudiness in the Garwood model, we have utilized the Stephens (1978) radiative scheme.

One of the important features of the Garwood model is its ability to consider the diurnal cycle. For example, the Kraus and Turner (1967) model uses daily averaged insolation. As the ocean-atmosphere interaction is so nonlinear, even in simple one-dimensional models, it is not clear whether the average solutions over a long period of time (of, say, SST

and mixed layer depths) will be the same as the equilibrium mixed layer structure using daily averaged insolation.

Even though we may understand how the changes in one flux at the ocean surface will effect the buoyancy of the upper ocean, the system is often forced by a combination of fluxes which makes the final outcome unclear. This is because certain sets of fluxes work in tandem. For example, the increase in buoyancy during a disturbed period due to a fresh water flux into the ocean may be offset by the decreased buoyancy from a reduction in solar radiation. The deep mixing accompanying a burst may be reduced by the increased solar radiation absorbtion in the upper layers. Such opposing effects make the tropical ocean region particularly sensitive and place very stringent requirements on models even if just the sign of changes in the upper ocean are all that are required. Table 3 shows the parameters which define the experiments used for the Garwood model.

Table 3

PARAMETERS FOR MIXED LAYER MODEL

	CASE	Fig.	V_s	τ_s	F_w	α_c	$\psi(z)$
1	Clear skies (days 0-14)	19 (a)	5	.6	-2.4	.25	10
	Cloudy (days 0-14)	19 (b)	5	.6	-2.4	.25	10
2	Shallow radiation attenuation (days (0-14)	19 (c)	5	.6	-2.4	.25	5
	Moderate radiation attenuation (days 0-14)		5	.6	-2.4	.25	10
	Deep radiation attenuation (days 0-14)		5	.6	-2.4	.25	20
3	Clear skies (0-7days) 5 m s^{-1}	19 (d)	5,	.6	-2.4	.25	10
	Clear skies (day 7-14) 15 m s^{-1}		15	1.8	-2.4	.25	10
4	Clear skies (day 0-7), ,	19 (e)	5	.6	-2.4	.25	10
	Cloudy, continuous rain (days 7-14)		5	.6	2.4	.5	10
	Clear, strong burst (days 14-21)		15	1.8	-2.4	.25	10

(a) Solar intensity and cloud: To study the impact of variations in solar intensity that accompany changes in cloud amount and type, the Garwood model, with the Stephens radiation scheme, was run for two 14–day periods using the parameters shown in the table.

Winds speeds were assumed to be light in both cases and an attenuation depth was set at 10 m. Albedos and emissivities corresponding to a liquid water path of 40 gm^{-2} were assumed.

Figure 19(a) shows diurnal "hysteresis" curves which show the mixed layer depth plotted against surface temperature. Both cases show a strong diurnal variation with shallower and warmer conditions in the afternoon. The deeper nocturnal mixed layers and cooler surface temperatures correspond to enhanced mixing from surface cooling. The effect of the reduced insolation was the cooling of the surface temperature. Although the diurnal variation of the "cloudy" curve is typical of the integration period, the case did not reach a final cyclic equilibrium as was rapidly achieved by the "clear" case. In fact, the surface temperature cooled at about .4°C or at a rate of 1°C/month which is very similar to Ramanathan's calculation using energy balance considerations, as discussed in Section 3.4. A plot of the SST and mixed layer depth evolution is shown in Fig. 19(b). Whereas it may be rare for the albedo to remian high for such a prolonged period, the results of the model confirm our expectations that cloud amount is an exceedingly important and sensitive quantity in the determining the ocean-atmosphere interaction. It would seem plausible that the interannual variation of cloudiness and the associated variation in the heating structure with depth associated with ENSO sea surface temperature variations could produce important feedbacks to the ocean structure.

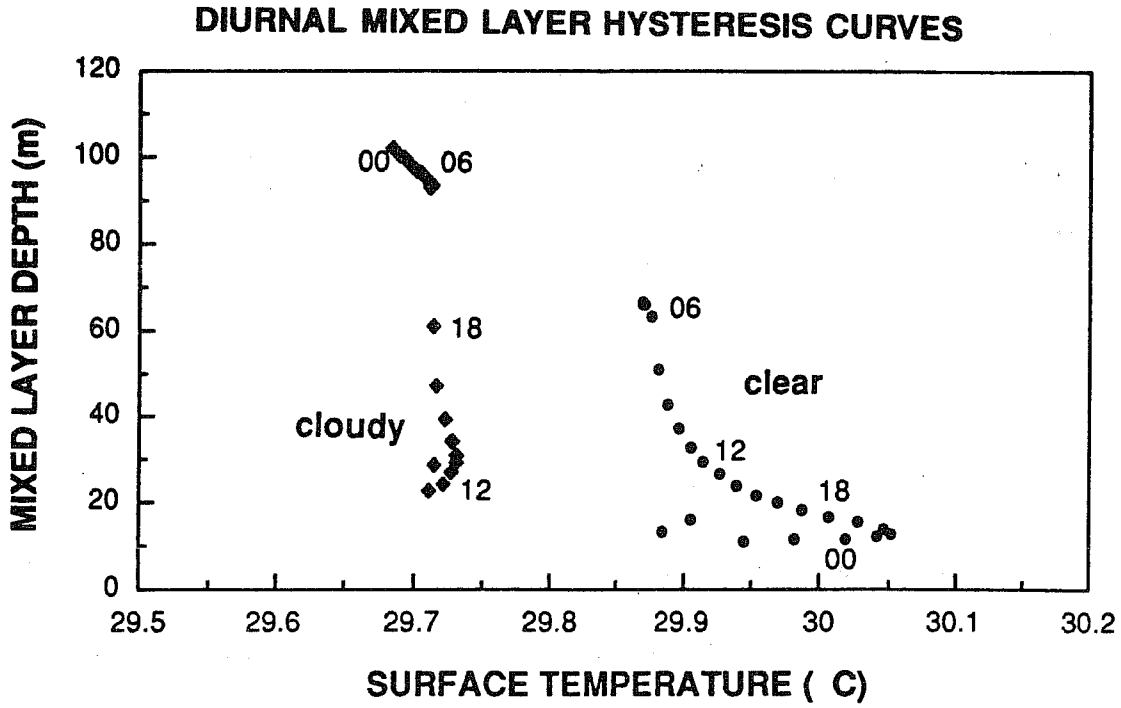

Figure 19(a): Comparison of the daily hysteresis curves of the mixed layer depth (density defined) and the sea surface temperature (SST) for relatively clear and cloudy conditions. The cloudy case assumes persistent fractional cloud which has an effective albedo of .5. Numbers indicate local time. Model parameters are listed in Table 3.

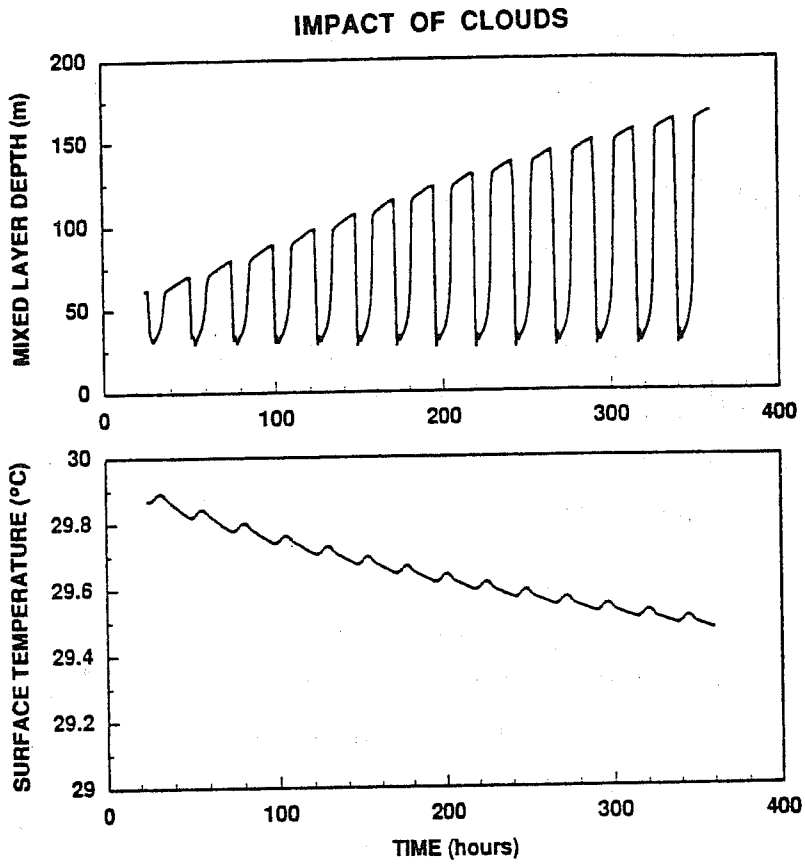

Figure 19(b): Time sequence of the mixed layer depth and SST for the cloudy case shown in Fig. 19 (b). Reduced insolation causes excessive cooling and deepening of the mixed layer. The cooling rate is about 1°C/month which is very similar to the estimates made by Ramanathan (1987) which is shown in Fig. 17.

(b) Radiational attenuation: Variations in attenuation depth can result for a number of reasons such as the variability of biological activity as a function of SST or insolation. Furthermore, there is some uncertainty as to what is the magnitude of the attenuation depth, its degree of spectral dependence and whether or not it varies regionally.

The first study to test the sensitivity of the ocean mixed layer to variations in the attenuation depth was made by Kraus and Turner (1967) using the original mixed layer model[10]. They used a simple attenuation coefficient for $\sum R$, thus ignoring the differential absorption of the radiation spectra and, thus, a major effect of clouds, and found an extreme sensitivity for the variation of the magnitude of the net radiational heating and the radiative attenuation. They showed that the predicted minimum depth of the summer extratropical thermocline was 80 m if the attenuation e-folding depth was 20 m but 57 m if the e-folding depth were changed to 10 m. Such variations in the net flux at the surface

[10] Kraus and Turner's model did not explicitly contain salinity. Unlike the Garwood model, Kraus and Turner's mixed layer depth was defined strictly in terms of temperature.

may be interpreted in terms of variations in the magnitudes of the individual streams by the variations of cloudiness.

To see if the Kraus-Turner sensitivity to attenuation depth also occurs in the tropics, three experiments were run with ψ_s set at 5, 10 and 20m, respectively. Time plots of the mixed layer depth and the SST are shown in Fig. 19(c). The diurnal variations are almost identical and only slight variations in the extrema are evident. With a smaller attenuation depth, the daytime mixed layer is shallower but the nocturnal cooling effectively eliminates differences. In the limited range of parameters considered here, it would appear that there is limited sensitivity to the variation of the mixed layer depth. This is a different result to that found by Kraus and Turner. Whether or not the discrepancies are due to model differences, experimental procedure (Kraus and Turner did not consider the diurnal cycle but used mean daily insolation and energy balances) or to real regional differences is unclear.

(c) Variations in wind stress associated with westerly bursts: Figure 19(c) shows the influence of a strong westerly burst on the structure of the upper ocean. On day 7 of the 14–day run, the wind speed at the ocean surface changes from 5 to 15 m s^{-1}, similar in magnitude to the speed changes observed in Figs. 13 and 14. The impact of the burst is very evident in both the depth and SST evolutions. With the burst, the mixed layer rapidly deepens and the SST cools substantially as the cooler sub-thermocline water is accessed.

(d) Impact of precipitation: A weather sequence in the western Pacific Ocean (Fig. 12) showed that there were distinct periods of disturbed weather over the warm pools of the western Pacific Ocean. Relatively clear periods would be followed by cloudy and rainy periods followed often by an intense westerly burst period. Figure 19(e) shows the impact of such a sequence on the upper ocean structure of a tropical warm pool. Following the clear period (identical to the situation shown in Fig. 19(a)) heavy steady rainfall occurs with overcast conditions. The decrease in insolation matches the situation shown in Fig. 19(b) but with a net 2.4 mm/hour fresh water flux. Finally at day 14, a 15 m s^{-1} westerly burst arrives which persists for the remainder of the experiment. With the precipitation and the reduced insolation (days 7–14), the mixed layer shallows as a fresh lens forms at the surface. However, the reduced insolation still causes a cooling of the surface layer. With the arrival of the burst, the mixed layer deepens relatively slowly at first but finally reaches depths similar to the burst case studied above. The transition period to the deeper mixed layer results from the finite time it takes for the burst to erode through the fresh lens. Thus, with this delay and the increase in insolation, the SST tend to rise after the burst arrives.

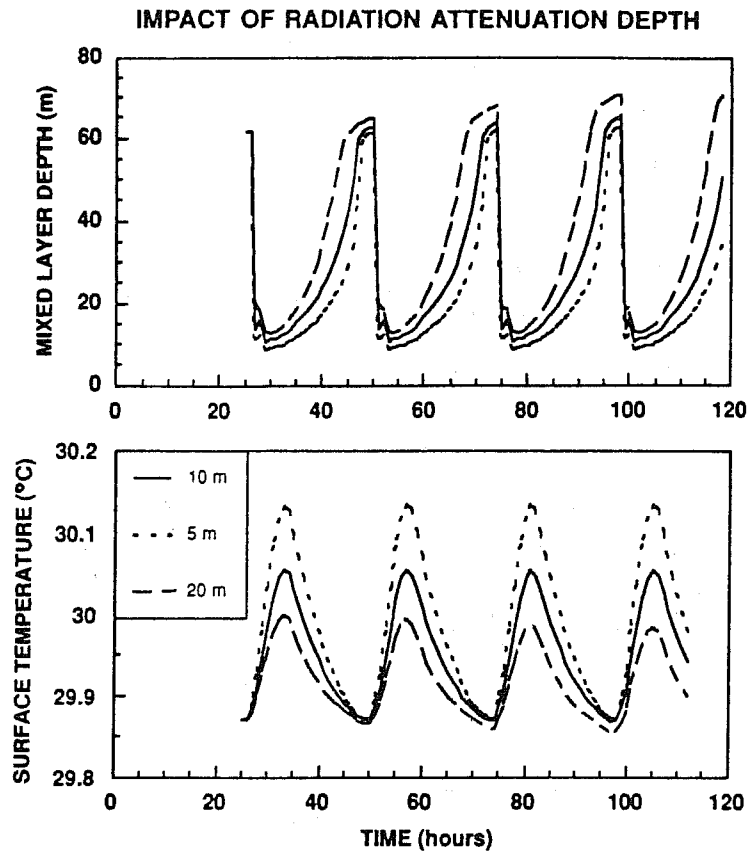

Figure 19(c): Time sequences of h and SST for three radiational attenuation depths of 5, 10, and 20 m. Garwood's model seems far less sensitive to the attenuation depth than the Kraus-Turner model.

However, surface cooling would resume if the burst were to continue or the mixed layer would progress to its pre-precipitation state if the winds were to lessen.

Lukas (1988) and Lukas and Lindstrom (1987) have speculated on the major importance of these competing aspects of the buoyancy flux in determining both the mean state of the tropical oceans and their interannual variability. Indeed, these processes form the basis of TOGA COARE.

4. EXTENSIONS TO LONGER TIME SCALES

On all time scales, the coupled ocean-atmosphere system is driven by the gradients of heating, especially in the latitudinal direction. Thus, the regions of ice and cold sea surface temperature, in conjunction with the maximum heating in the tropics, conspire to govern the overall climate of Earth. Below, we extend the argument one step further and propose a hypothesis which clearly involves the earth system as a robust interactive entity. The robustness refers to a resilient configuration of the climate. Within this scheme, the

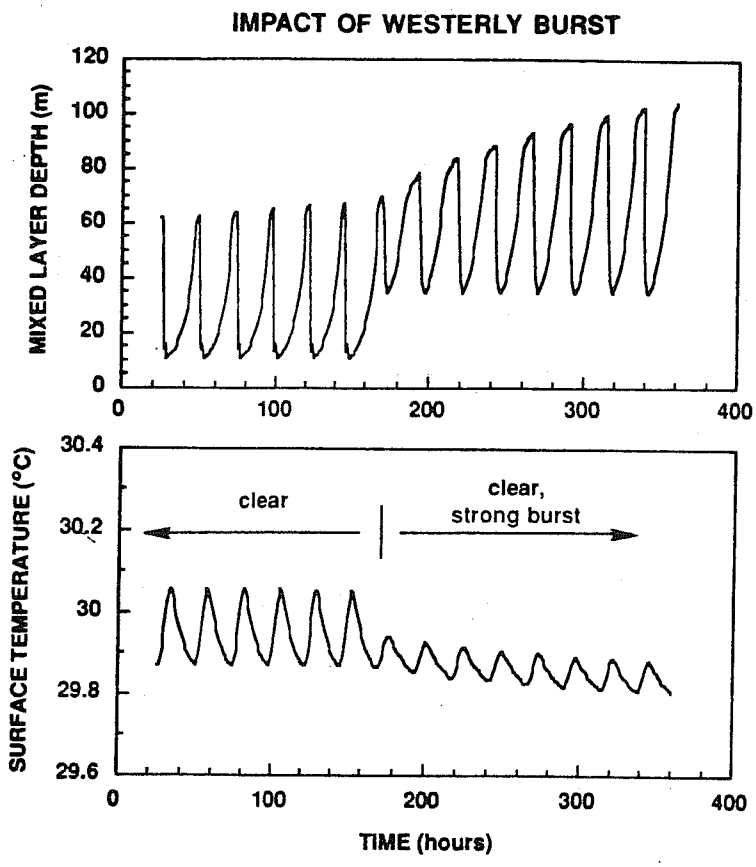

Figure 19(d): Impact on the ocean upper layer of a 15 m s^{-1} westerly wind bursts. Enhanced mixing causes substantial cooling as the diurnal mixed layer of the clear case is quickly eroded.

hydrology cycle, so important on interannual time scales, imparts a powerful constraint on the overall climate.

4.1 The Notion of Interactive Zones in the Ocean and the Atmosphere

In general, the ocean and the atmosphere have very different time scales. In a similar sense, the atmosphere has two zones with very different time scales, the troposphere and the stratosphere. The ocean two has also disparate temporal regimes; the slow deep ocean and a more rapid upper ocean. Figure 20(a) shows a different view of the coupled ocean-atmosphere system and proposes a linkage between the regions of diverse time scales.

As a working hypothesis, suppose that the regions of most rapid variability of the ocean and the atmosphere are those which interact together; namely, the upper region of the ocean and the whole troposphere. This interactive zone is demarked by the hatching in Fig. 20(a). Note that the interactive zone has a marked latitudinal structure. It is deepest in the atmosphere at low latitudes and in the ocean at high latitudes. The tropopause in the

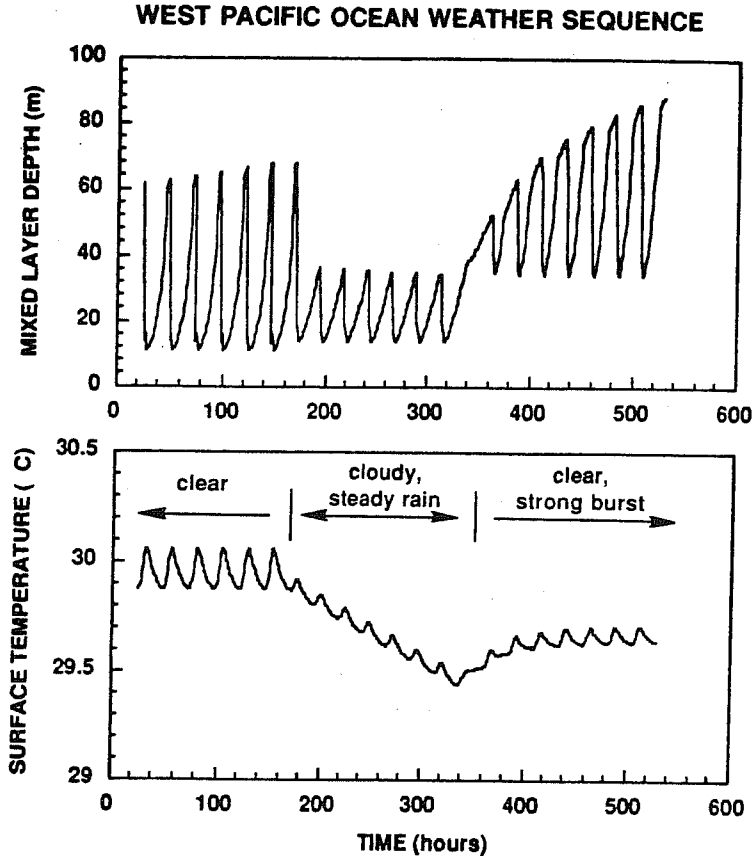

Figure 19(e): Response of the mixed layer to a sequence of weather events typical of the western Pacific Ocean. Following a clear period, persistent steady rainfall occurs for a seven-day period. During this time the reduced insolation dominates and the mixed layer cools although shallowing at the same time. The burst, set to occur on day 14, takes some time to erode through the fresh lens. Thus, initially a small warming occurs.

atmosphere separates the slow dynamics of the stratosphere from the rapid dynamics of the troposphere. Similarly, the thermocline separates the slow deep ocean from the more rapid upper ocean. In that sense, the tropopause and the thermocline fulfill the same roles in the ocean and the atmosphere, respectively, although they exist at different levels relative to the ocean-atmosphere interface. The tropopause lies at about 15-17 km in the tropics and at less than 10 km in the high latitudes. The depth of the troposphere is determined by the degree of convective penetration with the tropopause demarking the mean free convective height of the moist convection, which, in turn, is determined by the sea surface temperature as discussed in Section 2.1. The thermocline, on the other hand, lies below the surface at roughly 100 m in the tropics and probably extends to the ocean floor at higher latitudes. The depth of the thermocline (or its non-existence) corresponds to the region of the penetrative convection caused by the radiative cooling of the upper surface, the increase in salinity associated with ice formation and wind stress mixing. Thus, the tropical troposphere and the low latitude ocean are formed by similar processes: gravitational instability.

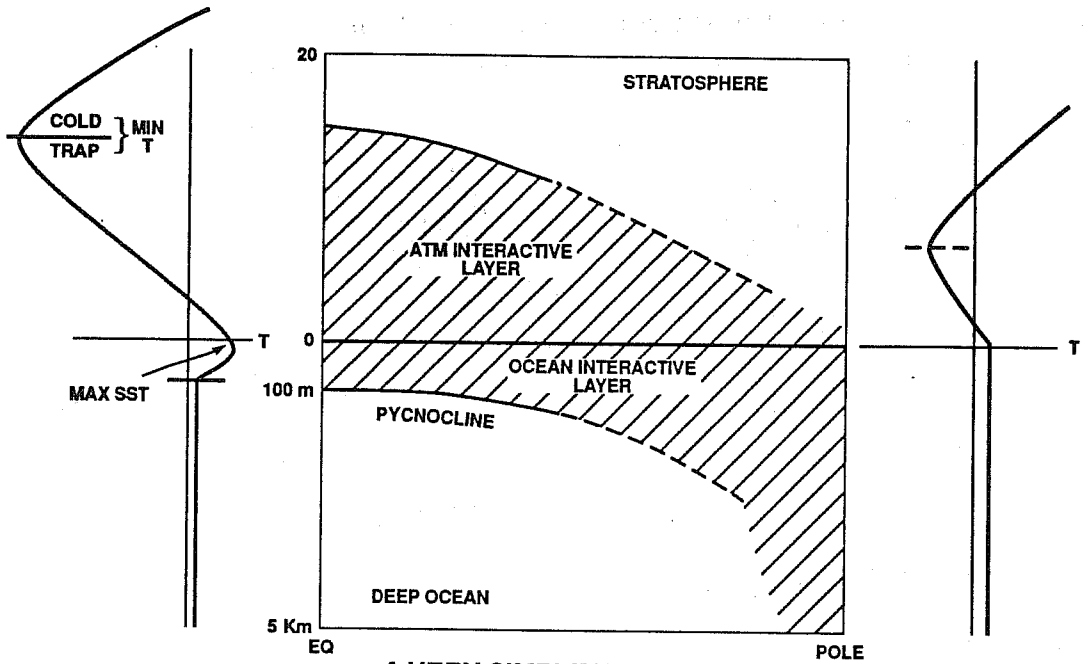

A VERY SIMPLE VIEW OF THE INTERACTIVE OCEAN-ATMOSPHERE SYSTEM

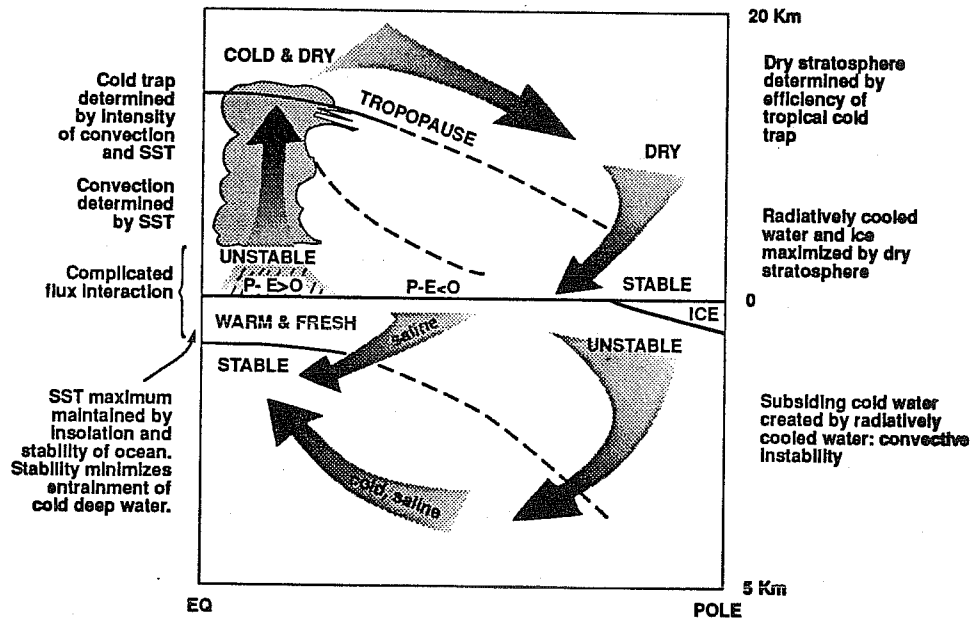

Figure 20: A very simple view of the interactive ocean-atmosphere system from a long-term and global perspective. (a) The interactive zones of the ocean and the atmosphere are the upper ocean and the troposphere. These regions denote the most rapidly evolving regions of the two spheres. The deep ocean below and the stratosphere above change on much longer time scales. (b) Through the interactive zones, the global system is maintained in firm equilibrium. In the tropics, complicated ocean-atmosphere fluxes and high insolation, and the very stable ocean configuration hold the SST in rather narrow bounds. The deep penetrative convection produces a very cold tropopause which provides a "cold trap" for moist air passing through to the stratosphere, thus assuring that the stratosphere remains dry. A cold, dry stratosphere assists the rapid cooling in the polar regions and the formation of cold saline deep water. The slow equatorial encroachment of the polar water, and the subduction of saline water below the equatorial warm pools, enhances the stability of the upper ocean structure at low latitudes and, thus, helps maintain the high temperature of the tropical water. In this manner, the ocean-atmosphere system,

4.2 A Hypothesis for an Interactive System

The similarity of the roles of the tropopause and the thermocline is not just happenstance. Fig. 20(b) shows a schematic diagram which attempts to put together the manner in which the ocean-atmosphere coexists. The figure shows a number of broad arrows which represent the circulations between the equator and the poles. Clearly, these are a response to the imposed radiational heating gradient. Notice that convection takes place in two parts of the system: in the tropical atmosphere (upwards) and the polar mixed layer (downwards). The convective (gravitational) instability is a result of very moist air over the warmest sea surface temperature. The convective instability in the polar oceans is caused by the intense radiational cooling at the surface of the ocean, ice formation and an effective negative buoyancy flux as salinity increases during the freezing process. Similar effects occur in the subtropics where strong evaporation causes ocean descent and the subduction of cool saline water under the equator. The tropical ocean mixed layer is very stable with rising cold water directed against gravity. Similarly, the polar atmospheric circulation is stable with descending and warming air producing a low level inversion. The warm SST and the tropical atmosphere determines the state of the upper atmosphere and the polar mixed layer in the ocean determines the deep water characteristics. Together, we find that the ocean and the atmosphere are, to a large degree, mirror images.

Within this very simplified model, Fig. 20(b) suggests that the SST gradient between the equator and the poles are self-regulated by the system and that a major regulator of the system is the hydrology cycle.

5. CONCLUSIONS AND GENERALIZATIONS

An attempt has been made to understand the role of hydrology over a wide range of space and time scales. Observational evidence indicated a wide range of convective phenomena. A combination of observations and theory indicated that the phenomena were tied to the ocean-atmosphere system. From the discussion, we may draw the following conclusions:

(a) The nonlinear relationship between saturation vapor pressure and temperature produces a strong regionality in the importance of the hydrology cycle. Saturation vapor pressure at temperatures 0°C, 10°C, 20°C and 30°C increase in the ratio of 1:1, :1.5, :3.5 and :10.0, respectively, relative to the saturation vapor pressure at 0°C. Thus, latent heating increases substantially at low latitudes and the latent heat fluxes from the warm

oceans increase in importance as the SST increases.

(b) The basic structure of the low latitude circulation is dominated by convective modes excited in the warm pool regions of the tropical oceans. In Section 2.1, it was suggested that these modes are both the most intense and possess the deepest structure. Furthermore, the warm pool regions are source regions of vigorous transients that influence other regions of the tropics and higher latitudes.

(c) Because of the latitudinal differences in water vapor concentration, especially in the planetary boundary layer, clouds change the total flux reaching the surface differently in the tropics and higher latitudes. Near the equator, where the ambient moisture concentrations are very high, the downwelling radiation is almost independent of cloud amount. At higher latitudes, the downwelling radiation compensates somewhat for the loss of solar radiation. Thus, clouds invoke a greater influence in the tropical regions in terms of net energy loss at the surface than at higher latitudes. One implication of the impact of clouds in the tropics is that the tropical upper ocean is considerably more sensitive to cloud amount than elsewhere.

(d) The warm pool regions of the tropical oceans are one of the few regions where precipitation exceeds evaporation by a large amount. For example, in the West Pacific, within the 28°C SST isopleth, *(P-E)* is greater than 2 m. This positive buoyancy flux effectively stabilizes the upper ocean producing a shallow mixed layer. The reduced mixing resulting from the increase in vertical stability of the ocean column allows for rapid heating. Only if the wind is very strong, such as occurs in equatorial westerly wind bursts, will the mixing be strong enough to erode through the stable fresh surface layer.

(e) Once convective modes are established over the warm pool regions, latent heating gradients are set up between the precipitating and dry regions. Simultaneously, identical gradients of net radiative flux convergence in a column are set up with magnitudes of about one third of the magnitude of the latent heating. Thus, latent heating and radiational heating gradients always have the same sign. However, the convergence of radiational flux in a cloudy region means that there will be a heating deficit in the ocean column below. Thus, once the latent and radiative heating gradients are established in the atmosphere, ocean cooling immediately commences in the ocean layer below the cloudy region and heating in the upper ocean below the less cloudy regions. Because

of the Clausius-Clapeyron relationship, small changes in the ocean temperature in the warmest regions will cause very large changes in the saturation vapor flux and in the latent heating gradient. The impact is to shift continually the region of warmest sea surface temperature along the equator and with it, the convection and clouds. The consequence of the feedback has yet to be explored. In this manner, the temperature of the tropical ocean is kept in bound by feedbacks from the hydrology cycle.

(f) Simple model calculations using the Garwood mixed layer model show the sensitivity of the coupled ocean-atmosphere system to imposed fluxes. The results are complicated because of compensations between processes which produce positive buoyancy fluxes (i.e., precipitation and radiational heating) and negative buoyancy fluxes (evaporation, radiational cooling). Model calculations suggest that, although radiational heating is diminished where strong precipitation occurs, the precipitation is usually so intense that the mixed layer shallows considerably. However, when there are westerly bursts there is usually a solar heating maximum. In this case, as the upper ocean is particularly stable because of the fresh lens produced by subsequent precipitation, only the very strongest winds will erode through the barrier layer and cool the surface.

In order to account for the interactive hydrology cycle in an adequate manner, modelers are faced with some difficult problems. The problems increase substantially when attempts are made to model the coupled system. In the tropical atmosphere, there is a premium on modeling clouds properly where it is very important that cloud amount be specified correctly. Thus, at low latitudes, the most important property is the adequate description of the magnitude of the solar radiation at the surface. In that case, cloud amount is more important than cloud height. However, at higher latitudes, all aspects of the cloud are necessary as the downwelling long-wave radiation becomes more variable.

The principal aim of the TOGA Programme is to assess the predictibility of the climate system on interannual time scales. The ultimate tool to be used in this ambitious program is the coupled ocean-atmosphere model. Clearly, the most straightforward way to assess the importance of some of the processes discussed above is through numerical experimentation. The observations gathered from the remote systems or from the field experiments couple well with the model development. In order to improve parameterization schemes, considerably more data on the water budget of the earth system is necessary. Currently, we probably know quantities such as area-averaged precipitation only to within a factor of two and surface energy balances to a not much better accuracy. Clearly, given the discussion above,

a high priority must be ascribed to the satellite determination of precipitation. Active and passive microwave radiometers, such as those planned for TRMM (the Tropical Rainfall Measurement Mission), will hopefully provide estimates of area averaged rainfall to within a few percent averaged over one month, easily fulfilling TOGA requirements. Furthermore, the satellite will also allow cloud structure and hydrometer distribution to be measured for the first time on a tropics wide basis which will provide data to aid in the determination of subcloud layer radiation fluxes. However, such space experiments must be coupled with carefully designed ground truth experiments and modeling programs.

Observations from space are probably only as good as those from the ground. Ground truth observations may come from such endeavors as TOGA COARE (Coupled Ocean-Atmosphere Response Experiment). Aimed ostensibly at understanding the maintenance of the warm ocean regions, the large scale convection-sea surface temperature relationships and the response of the ocean to episodic forcing through convective events and westerly burst phenomena, the experiment offers the opportunity for the determination of flux structure through the coupled system for an extended period over a large and important region of the tropics.

Many of the activities discussed in this section are already underway. Observational satellite systems that will approach many of the objectives described are being planned. For example, the TRMM experiment is undergoing active development. The international scientific community are considering the design of the next generation of satellites that will provide global coverage of the hydrology cycle for the Global Energy and Water Experiment (GEWEX).

Acknowledgments: The research in this paper has been supported by the National Science Foundation under Grant ATM 87–03267 and by the National Oceanographic and Atmospheric Administration under Grant NA89AA–D–AC015. Many of the ideas that are present in the manuscript arise from the development of the TOGA COARE program. I would like to thank Prof. Roger Lukas and members of my group, in particular, Dr. Song Yang, for many interesting discussions. Special thanks are due to Dr. Judith Curry for her suggestions regarding the manuscript. I also appreciate the kindness of Dr. Garwood for making available the ocean mixed layer model.

References

Arkin, P., and P. J., Webster, 1985: Annual and interannual variability of the tropical-extratropical interaction: An imperical study. *Mon. Wea. Rev., 113*, 1510-1523.

Bjerknes, J., 1969: Atmospheric teleconnections from the equatorial Pacific. *Mon. Wea. Rev., 97*, 163-172.

Chang, C. P., 1977: Viscous internal gravity waves and low frequency oscillations in the tropics, *J. Atmos. Sci., 34*, 901-910.

Chang, H–. R. and P. J. Webster, 1990: Energy accumulation and emanation at low latitudes. Part II: Nonlinear response to strong episodic forcing. *J. Atmos. Sci.*, 47 November.

Garwood, R. W., 1977: An ocean mixed layer model capable of simulating cyclic states. *J. Phys. Oceanogr.*, 7, 455–468

Garwood, R. W., P. Muller, and P. C. Gallacher, 1985: Wind direction and equilibrium mixed layer depth in the tropical Pacific Ocean *J. Phys. Oceanogr.*, 7, 455–468

Gill, A., 1980: Some simple solutions for heat induced tropical circulations, *Quart. J. Roy. Met. Soc, 106*, 447-462.

Godfrey, J. S., 1990: A strategy for TOGA salinity monitoring, Proceedings of Workshop on Japenese Coupled Ocean Atmosphere Response Experiments, 23–24, October, 1989, *Meteorological Research Report*, Division of Meteorology, Geophysical Institute, University of Tokyo, 90–2.

Hoskins, B., and D. Karoly, 1982: The steady linear response of a spherical atmosphere to thermal and orographic forcing. *J. Atmos. Sci., 38*, 1179-1196.

Knox, R. A., and D. Halpern, 1982: Long range Kelvin wave propagation of transport variations in the Pacific Ocean equatorial currents. *J. Mar. Res. 40*, (suppl), 329-339.

Kraus, E., and S. Turner, 1967: A one-dimensional model of the seasonal thermocline: II The general theory and its consequences. *Tellus, 19*, 98-106.

Krishnamurti, T. N., 1971:Tropical east-west circulations during the northern hemisphere summer. *J. Atmos. Sci, 28*, 1342-1347.

Lau, K. –M., and P. H. Chan, 1988: Intraseasonal and interannual variations of tropical convection: a possible link between the 40–day mode and ENSO, *J. Atmos. Sci.*, 45, 950–972

Lau, K. –M., L. Peng, C. H. Sui and T. Nakazawa, 1988: Dynamics of multisclae interactions associated with the westerly wind burst, super cloud clusters, 30–60 day oscillations and ENSO. Submitted to *J. Met. Soc. Japan*

Leathers, D., 1986: Edge wave characteristics of East Asian Cold Surges, Master of Science Thesis, Department of Meteorology, The Pennsylvania State University, 108 pp.

Love, G, 1985: Cross-equatorial influence of winter hemisphere subtropical cold surges. *Mon. Wea. Rev, 113*, 1487-1509.

Lukas, R. and E. Lindstrom, 1987: The mixed layer of the western equatorial Pacific ocean. In Proceedings of the 'Aha Huliko'a Hawaiin Winter Workshop on the Dynamics of the Oceanic Surface Mixed Layer, Honolulu, Hawaii, P. Muller and D. Henderson, eds., Hawaii Institute of Geophysics Special Pub., pp 67–94.

Lukas, R. 1988: On the role of western Pacific air-sea interaction in the El Niño/Southern Oscillation phenomena, Proceedings of the U.S. TOGA Western Pacifc Air-Sea Interaction Workshop, (eds., R. Lukas and Peter J. Webster), pp 43–69.

Luther, D.S., Harrison, E., and R. Knox, 1983: Zonal winds in the central equatorial Pacific Ocean and El Niño. *Science*, 222 327-330.

Nakazawa, T., 1988: Tropical superclusters under intraseasonal variation, Proceedings; Japan-U.S., Workshop on the ENSO Phenomena, University of Tokyo, Nov. 3–7, 1987, Meteorological Research Report, #88–1, Department of Meteorology, Geophysical Institute, 76–78.

Palmer, T. N., and D. A. Mansfield, 1984: Response of two general circulation models to sea-surface temperature anomalies in the tropical East and West Pacific. *Nature 310*, , 483–485.

Philander, S. G. H., 1989: El Niño, La Niña and the Southern Oscillation, Academic press, 283 pp

Oberhuber, J. M., 1988: An Atlas Based on the COADS data set: The Budgets of Heat, Buoyancy and Turbulent kinetic Energy at the Surface of the Global Ocean, Report No. 15, Max-Plank-Institut, Hamburg, 20 pp, 160 Figs..

Opsteegh, J.D. and H.M. van der Dool, 1980: Seasonal differences in the stationary response of a linearized primitive equation model: Prospects for long-range forecasting? *J. Atmos. Sci., 37.*

Ramanathan, V., 1987: Atmospheric general circulation and its low frequency Variance:Radiative Influences. *J. Met. Soc. Japan*, (in press).

Sardeshmukh, P. D. and B. J. Hoskins, 1988: The generation of global rotational flow by steady idealized tropical divergence. *J. Atmos. Sci., 35*,, 45, 1228–1251

Sellers, W. D., 1972: Physical Climatology, The University of Chicago Press, 272pp

Sikka, D. and S. Gadgil, 1980: On the maximum cloudiness zone and the ITCZ over Indian longitudes during the Southwest Monsoon, *Mon. Wea. Rev.*,, **108**, 1840–1853.

Shukla, J. and Y. Mintz, 1982, The influence of land evapotranspiration on Earth's climate, *Science*, **215**, 1498–1501.

Simpson, J. J. and T. D. Dickey, 1981: The relationship between downward irradiance and upper ocean structure, *J. Phys. Ocean., 11*, 309-323.

Srinivasan, J., S. Gadgil and P. J. Webster, 1990: Meridional Propagation of Large-scale convective zones, submitted to *J. Geophys. Res; Atmosphere*,

Stephens, G. L., 1978: Radiative properties of extended water clouds: II Parameterizations. *J. Atmos. Sci., 35*, 2133-2142.

Stephens, G.L. and P. J. Webster, 1979: Cloud and climate: Sensitivity of simple systems. *J. Atmos. Sci., 38* ,235-247.

Stephens, G. L., and P. J. Webster, 1983: Cloud decoupling of surface and upper radiation balances. *J. Atmos. Sci., 41*, 681-686.

Webster, P. J., 1972: Response of the tropical atmosphere to local steady forcing. *Mon. Wea. Rev., 25, 100*, 518-540.

Webster, P. J., 1973: Temporal Variation of low latitude zonal circulations. *Mon. Wea. Rev, 101*, 803-816.

Webster, P. J., 1982: Mechanisms determining the response to sea surface temperature anomalies, *J. Atmos. Sci., 38*, 554-571

Webster, P. J., 1983: Seasonality in the local and remote response to sea surface temperature anomalies. *J. Atmos. Sci., 39*, 41-52.

Webster, P. J., 1987: The Interactive Monsoon, In Monsoons, J. S. Fein and P. L. Stephens, editors. Wiley-Interscience, 269–330..

Webster, P. J. and H-. R. Chang, 1987: Equatorial energy accumulation and emanation regions: Impacts of a zonally varying basic state. to appear in *J. Atmos. Sci.* (February, 1988).

Webster, P. J. and J. R. Holton, 1982: Cross equatorial response to mid-latitude forcing in a zonally varying basic state, *J. Atmos. Sci., 39*, 722-733.

Williams, M., 1981: Interhemispheric interaction during Winter MONEX. *Proceedings International Conference on the Early Results of FGGE and the Large-scale Aspects of its Monsoon Experiments*, W.M.O., 10:12-16.

Woods, J. D. 1984: The upper ocean and air-sea interaction in global climate. Chapter 9: *The Global Climate*, (editor John J. Houghton), Cambridge University Press, Cambridge.

Yang, S., and Peter J. Webster, 1990: The intensity of the Asian Summer Monsoon Circulation and the Longitudinal Heating Gradient, submitted to *J. Climate*,